nature cell biology

Article

https://doi.org/10.1038/s41556-024-01351-9

ECSIT facilitates memory CD8$^+$ T cell development by mediating fumarate synthesis during viral infection and tumorigenesis

Received: 7 February 2023

Accepted: 7 January 2024

Published online: 7 February 2024

Check for updates

Yongbing Yang[1,2,7], Yanan Wang[1,7], Zhongcheng Wang[3], Huanyu Yan[4], Yi Gong[1], Yingchao Hu[1], Yuying Jiang[1], Shuang Wen[1], Feifei Xu[3], Bingwei Wang[5], Fiachra Humphries[6] ✉, Yun Chen[3] ✉, Xi Wang[4] ✉ & Shuo Yang[1] ✉

Memory CD8$^+$ T cells play a crucial role in infection and cancer and mount rapid responses to repeat antigen exposure. Although memory cell transcriptional programmes have been previously identified, the regulatory mechanisms that control the formation of CD8$^+$ T cells have not been resolved. Here we report ECSIT as an essential mediator of memory CD8$^+$ T cell differentiation. Ablation of ECSIT in T cells resulted in loss of fumarate synthesis and abrogated TCF-1 expression via demethylation of the TCF-1 promoter by the histone demethylase KDM5, thereby impairing memory CD8$^+$ T cell development in a cell-intrinsic manner. In addition, ECSIT expression correlated positively with stem-like memory progenitor exhausted CD8$^+$ T cells and the survival of patients with cancer. Our study demonstrates that ECSIT-mediated fumarate synthesis stimulates TCF-1 activity and memory CD8$^+$ T cell development during viral infection and tumorigenesis and highlights the utility of therapeutic fumarate analogues and PD-L1 inhibition for tumour immunotherapy.

Memory CD8$^+$ T cells play a crucial role in mounting a rapid immune response to eliminate reinfection[1,2]. When presented with antigens, naive CD8$^+$ T (T_N) cells undergo an initial activation step, followed by expansion to generate effector CD8$^+$ T cells that eliminate pathogens and tumour cells[1,3,4]. At the peak of the response, CD8$^+$ T cells exist as differing differentiation states ranging from short-lived effector cells (SLECs) to long-lived memory-precursor effector cells (MPECs)[5]. SLECs (CD127^{lo}KLRG1^{hi}) differentiate into short-lived effector CD8$^+$ T cells and exhibit potent cytotoxicity. MPECs (CD127^{hi}KLRG1^{lo}) differentiate further into long-lived mature memory CD8$^+$ T cells to confer durable immunity[5,6].

CD8$^+$ T cells often differentiate into a dysfunctional state as a result of 'T cell exhaustion' during chronic infection. Recent studies

[1]Department of Immunology, State Key Laboratory of Reproductive Medicine, Jiangsu Key Lab of Cancer Biomarkers, Prevention and Treatment, Collaborative Innovation Center for Personalized Cancer Medicine, Gusu School, the Affiliated Wuxi People's Hospital of Nanjing Medical University, Wuxi People's Hospital, Wuxi Medical Center, National Vaccine Innovation Platform, School of Basic Medical Sciences, Nanjing Medical University, Nanjing, China. [2]Department of Medical Laboratory, Affiliated Children's Hospital of Jiangnan University, Wuxi, China. [3]School of Pharmacy, Nanjing Medical University, Nanjing, China. [4]State Key Laboratory of Reproductive Medicine, Nanjing Medical University, Nanjing, China. [5]Department of Pharmacology, Nanjing University of Chinese Medicine, Nanjing, China. [6]Division of Innate Immunity, Department of Medicine, UMass Chan Medical School, Worcester, MA, USA. [7]These authors contributed equally: Yongbing Yang, Yanan Wang. ✉e-mail: Fiachra.Humphries@umassmed.edu; ychen@njmu.edu.cn; xiwang@njmu.edu.cn; shuoyang01@njmu.edu.cn

have shown that the pool of exhausted CD8$^+$ T cells is developmentally and functionally heterogeneous, incorporating terminally exhausted cells co-expressing high levels of PD-1 and TIM-3, and stem-like memory progenitor exhausted T cells ($T_{SM\text{-}PEX}$) that express T cell factor 1 (TCF-1) and stem cell antigen-1 (SCA-1) but lack expression of TIM-3, having features resembling memory cells[7,8]. TCF-1^{hi} $T_{SM\text{-}PEX}$ cells maintain the quality of long-term self-renewal, which replenishes terminally exhausted TCF-1^{low} populations, and TCF-1$^+$PD-1$^+$ tumour-infiltrating lymphocytes mediate the response to immunotherapy[9,10].

Transcriptional programmes regulate the fate of CD8$^+$ T cells such as short-lived cytotoxic effectors, long-lived self-renewing memory cells, terminally exhausted and $T_{SM\text{-}PEX}$ cells. TCF-1 (ref. 11), BCL-6 (ref. 12) and ID-3 (ref. 13) drive gene expression programmes of long-lived memory cells and $T_{SM\text{-}PEX}$ cells. BLIMP-1 (refs. 14,15) and T-BET[15] induce transcriptional programmes required for SLEC differentiation, whereas NR4A[16] and TOX[17] promote the formation of terminally exhausted subpopulations. Note that the TCF-1-centred transcriptional network plays a master regulatory role in generating the CD8$^+$ T cell memory response[11,18]. However, the regulatory mechanisms underlying the activity of TCF-1 remain largely unknown.

Evolutionarily conserved signalling intermediate in Toll pathways (ECSIT) was originally reported as an essential protein in mesoderm formation, NFκB activity, mitochondrial reactive oxygen species (mROS) production, mitophagy and complex I assembly, cardioprotection and intestinal cell development[19–25]. The role of ECSIT in adaptive immunity is still unclear. Notably, we identified ECSIT expression in immune cells to be significantly enriched in T cells, particularly memory CD8$^+$ T cells (Fig. 1a–c). Thus, we evaluated ECSIT function in memory CD8$^+$ T cells.

Here we report that ECSIT is essential for the differentiation and function of memory CD8$^+$ T cells. Deletion of ECSIT leads to metabolic changes that result in a loss of fumarate and impaired TCF-1 activity accompanied with demethylation of trimethylation of histone H3 at lysine 4 (H3K4me3) modifications the TCF-1 promoter.

Results

ECSIT expression is enriched in memory CD8$^+$ T cells

Ecsit is abundantly expressed in memory CD8$^+$ T cells (Fig. 1a,b). In particular, *Ecsit* was enriched in long-lived central memory and $T_{SM\text{-}PEX}$ cells in lymphocytic choriomeningitis virus (LCMV) infection and the tumour microenvironment (TME; Fig. 1c). We generated *Ecsit*–EGFP reporter mice to monitor the *Ecsit* expression of CD8$^+$ T cell subpopulations (Supplementary Fig. 1a). *Ecsit* expression levels in *Ecsit*–EGFP mice were confirmed to be significantly higher in CD8$^+$ T cells compared with myeloid, B, natural killer (NK) and CD4$^+$ T cells (Fig. 1d and Extended Data Fig. 1a). Furthermore, *Ecsit* expression was higher in central memory CD8$^+$ T cells (T_{CM}) compared with CD8$^+$ T_N and effector memory T (T_{EM}) cells under homeostatic conditions (Fig. 1e and Extended Data Fig. 1b). In addition, *Ecsit* was abundant in MPECs and CD8$^+$ T_{CM} cells infected with vesicular stomatitis virus encoding OVA (VSV-OVA; Fig. 1f,g and Extended Data Fig. 1c,d). In a B16F10 melanoma engraftment model *Ecsit* expression was markedly higher in $T_{SM\text{-}PEX}$ cells than terminally exhausted T cells (T_{EXH}; Fig. 1h and Extended Data Fig. 1e). Thus, ECSIT is abundantly expressed in memory CD8$^+$ T cells.

ECSIT deficiency impairs the generation of memory CD8$^+$ T cells in a cell-intrinsic manner in vivo

We first crossed *Ecsit*$^{fl/fl}$ mice with mice expressing Cre recombinase under the control of distal Lck promoter (*dLck*-Cre)[26]. *dLck*-Cre activity only occurs after the positive selection of thymocytes in adult mice (Supplementary Fig. 1b–d). Intercrossing of *Ecsit*$^{fl/fl}$ with *dLck*-Cre mice resulted in the deletion of ECSIT on CD4$^+$ and CD8$^+$ T cells in peripheral lymphoid organs (Supplementary Fig. 1e). The proportions of thymic T cells remained comparable between *Ecsit*$^{fl/fl}$ and *Ecsit*$^{fl/fl}$ *dLck*-Cre mice (Supplementary Fig. 2a,b). However, we observed a significant specific reduction in CD8$^+$ T cells as well as the frequency of memory CD44$^+$CD62L$^{+/-}$ CD8$^+$ T cells (T_M) and a concomitant increase in CD44$^-$CD62L$^+$ CD8$^+$ T_N cells in the peripheral lymphoid organs and blood of *Ecsit*$^{fl/fl}$ *dLck*-Cre mice in comparison to the *Ecsit*$^{fl/fl}$ controls (Supplementary Fig. 2c–j).

We next performed mixed bone marrow adoptive transfer experiments using bone marrow cells from *Ecsit*$^{fl/fl}$ or *Ecsit*$^{fl/fl}$ *dLck*-Cre (CD45.2$^+$) mice mixed at a 1:1 ratio with cells from wild-type (WT) B6.SJL (CD45.1$^+$) mice. The WT and *Ecsit*$^{fl/fl}$ or *Ecsit*$^{fl/fl}$ *dLck*-Cre T cells developed and were homeostatically maintained in the same in vivo environment. Following mixed bone marrow adoptive transfer, a marked decrease in CD8$^+$ T cells, particularly T_M cells, was observed in the spleen and draining lymph nodes of the ECSIT-deficient T cell model in comparison to the control (Fig. 1i and Extended Data Fig. 1f), thus suggesting a T cell-intrinsic indispensable role of ECSIT for the generation of memory phenotype CD8$^+$ T cells under homeostatic conditions.

ECSIT deletion attenuates the recall response of antigen-specific CD8$^+$ T cells

To study the function of ECSIT in antigen-specific T cells, we generated *Ecsit*$^{fl/fl}$ *dLck*-Cre OT-1 T cell antigen receptor (TCR) transgenic mice, which enables the development of CD8$^+$ T cells specific for the Kb-ovalbumin $(OVA)_{257–264}$ epitope[27]. We injected an equal number of *Ecsit*$^{fl/fl}$ OT-1 (WT) or *Ecsit*$^{fl/fl}$ *dLck*-Cre OT-1 (knockout, KO) T_N cells into WT recipient mice, followed by infection with VSV-OVA. The percentage and number of MPECs decreased in ECSIT-deficient mice but no significant changes were observed for SLECs at the early stage of viral infection (Supplementary Fig. 3a,b). Proliferation and apoptosis were unaffected (Supplementary Fig. 3c,d).

We next employed OVA-specific T cells to determine antigen-specific memory CD8$^+$ T cells. We heterogeneously rechallenged host mice harbouring VSV-OVA-induced WT or KO OT-1 memory CD8$^+$ T cells with a different pathogen carrying the same antigen—*Listeria monocytogenes* expressing ovalbumin (LM-OVA)—and then measured their recall response (Extended Data Fig. 2a). The recall responses of ECSIT-deficient memory T cells in the spleen and liver were markedly impaired, as demonstrated by a higher colony burden, substantial reduction in OVA-specific CD8$^+$ T cells and significantly decreased levels of both interferon γ (IFN-γ$^+$)- and tumour necrosis factor α (TNF-α$^+$)-producing cells (Extended Data Fig. 2b–i). These data suggest that ECSIT in T cells is required to maintain the functional identity of memory CD8$^+$ T cells.

Cell-intrinsic requirement of ECSIT for memory T cell formation and the function of antigen-specific CD8$^+$ T cells in response to acute viral infection

We next used a mouse line carrying a Cre-oestrogen receptor T2 (CreERT2) allele in the ROSA26 locus (*Rosa26*^{CreERT2}) that can temporally control ECSIT expression and is activated by tamoxifen. We generated *Ecsit*$^{fl/fl}$ *Rosa26*^{CreERT2} OT-1 mice, and sorted congenically marked OT-1 T_N cells from *Ecsit*$^{fl/fl}$ *Rosa26*^{CreERT2} OT-1 and *Ecsit*$^{fl/fl}$ OT-1 control mice and transferred them into B6 mice separately, which were then infected with VSV-OVA. Tamoxifen was administered to induce ECSIT deletion during the late stages of memory T cell development (Extended Data Fig. 2j and Extended Data Fig. 3a). The deletion of ECSIT during the formation of memory T cells by VSV-OVA infection led to a reduction in OVA-specific CD8$^+$ T cells and decreased IFN-γ and TNF-α production (Fig. 2a–c and Extended Data Fig. 3b–d), with no effect on cell death or proliferation (Extended Data Fig. 3e,f). Splenic MPECs and the expression of the memory T cell marker CD62L were significantly decreased, whereas the percentage of SLECs and the expression of the effector molecule CD44 was significantly increased (Fig. 2d,e and Extended Data Fig. 3g), thus confirming that ECSIT controls the differentiation of memory CD8$^+$ T cells in response to viral infection. Moreover, the expression levels of the memory-associated transcription factors TCF-1 (ref. 11), FOXO-1 (ref. 28) and BCL-6 (ref. 12) were significantly reduced

https://doi.org/10.1038/s41556-024-01351-9

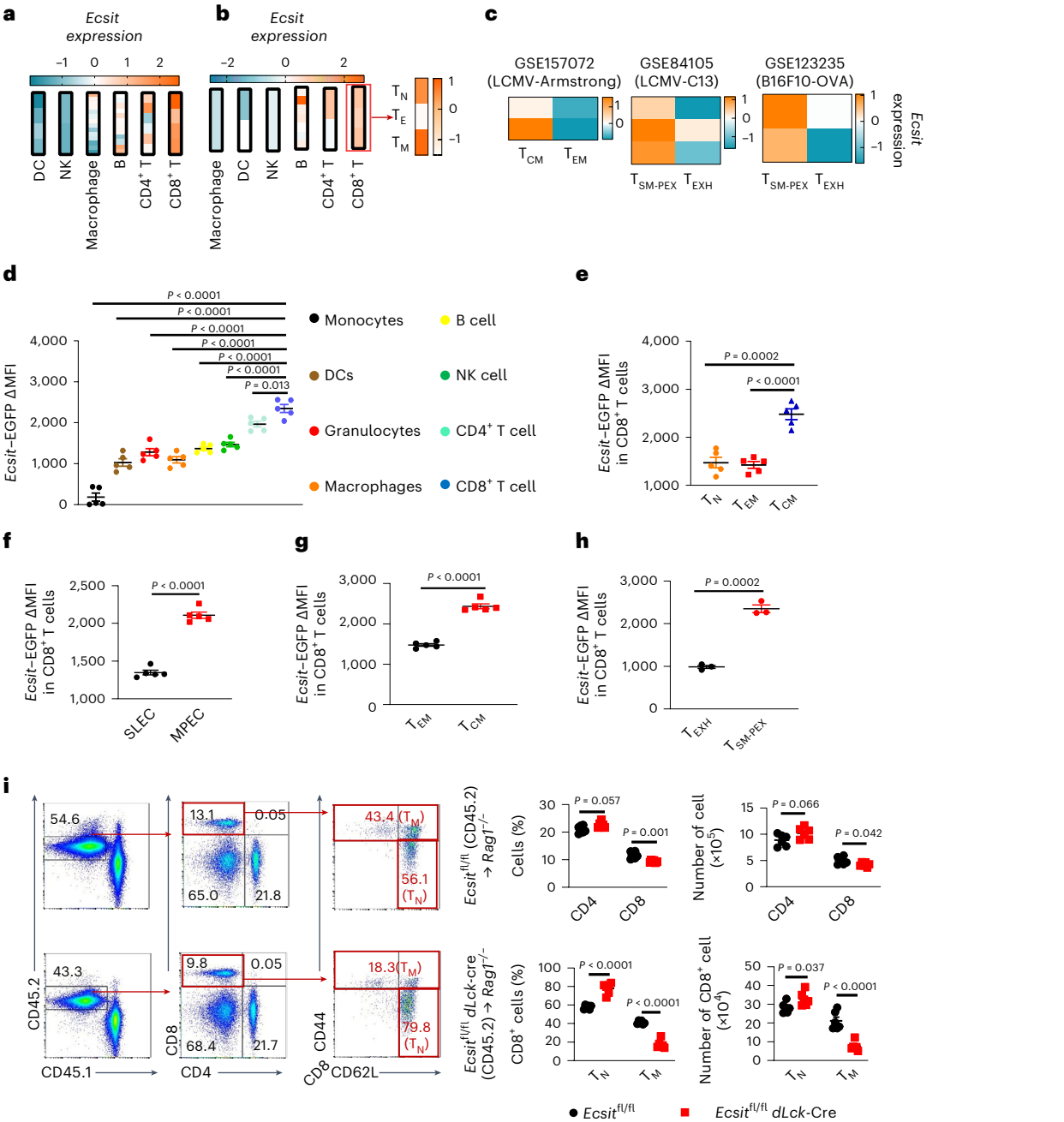

Fig. 1 | ECSIT is upregulated in memory CD8⁺ T cells and promotes memory CD8⁺ T cell generation in a cell-intrinsic manner under homeostasis. **a**, *Ecsit* expression levels in mouse immune cells from the publicly available gene database BioGPS (http://biogps.org/). **b**, *Ecsit* expression levels in mouse immune cells from the publicly available gene database ImmGen (https://www.immgen.org/). The red box demonstrates the isolation of the original *Ecsit* expression data in mouse CD8⁺ T cells from the ImmGen database to re-analyse and re-calculate the *Z*-score value of naïve T_N, T_M and T_E cells. The orange scale bar shows the *Z*-score value of the *Ecsit* expression in mouse CD8⁺ T cells from the ImmGen database. **c**, *Ecsit* expression levels in T_{CM} and T_{EM} (left; from the publicly available Gene Expression Omnibus (GEO) accession number GSE157072), and $T_{SM\text{-}PEX}$ and T_{EXH} (middle and right; GEO accession numbers GSE84105 and GSE123235) cells. **d**, Flow cytometry analysis of mouse *Ecsit*–EGFP expression in monocyte cells (CD45⁺CD11b⁺Ly6C⁺Ly6G⁻), dendritic cells (DCs; CD45⁺CD11c⁺MHC-II⁺), granulocytes (CD45⁺CD11b⁺Ly6G⁺Ly6C⁻), macrophages (CD45⁺CD11b⁺F4/80⁺), B cells (CD45⁺CD19⁺), NK cells (CD45⁺NK1.1⁺), CD4⁺ T cells (CD45⁺TCR-β⁺CD4⁺) and CD8⁺ T cells (CD45⁺TCR-β⁺CD8⁺) in homeostasis. **e**, Flow cytometry analysis of *Ecsit*–EGFP expression in T_N (CD8⁺CD62L⁺CD44⁻), T_{CM} (CD8⁺CD62L⁺CD44⁺) and T_{EM} (CD8⁺CD62L⁻CD44⁺) subsets of mouse CD8⁺ T cells in homeostasis. **f**,**g**, Flow cytometry analysis of *Ecsit*–EGFP expression in MPECs (CD8⁺CD127⁺KLRG1⁻) and SLECs (CD8⁺CD127⁻KLRG1⁺) (**f**) as well as T_{CM} and T_{EM} subsets (**g**) of the CD8⁺ T cells of *Ecsit*–EGFP mice infected with VSV-OVA. **h**, Flow cytometry analysis of *Ecsit*–EGFP expression in CD8⁺ $T_{SM\text{-}PEX}$ (CD8⁺PD-1⁺TIM-3⁻SCA-1⁺) and T_{EXH} (CD8⁺PD-1⁺TIM-3⁺) cells of B16F10 tumour-bearing *Ecsit*–EGFP mice. **i**, Bone marrow from CD45.1 mice was mixed with equal amounts of $Ecsit^{fl/fl}$ or $Ecsit^{fl/fl}$ *dLck*-Cre (CD45.2) mouse bone marrow and then intravenously (i.v.) injected into irradiated $Rag1^{-/-}$ mice. After 8 weeks the mouse spleens were collected and analysed by flow cytometry for CD4⁺ T, CD8⁺ T and CD8⁺ T_N and T_M cells. A representative analysis is shown with the percentage of cells in the relevant quadrants indicated (left). **d**–**i**, Data were pooled from three independent experiments; $n = 5$ for (**d**–**g**), 3 (**h**) and 6 (**i**); data are the mean ± s.e.m. Two-tailed unpaired Student's *t*-test. MFI, mean fluorescence intensity.

https://doi.org/10.1038/s41556-024-01351-9

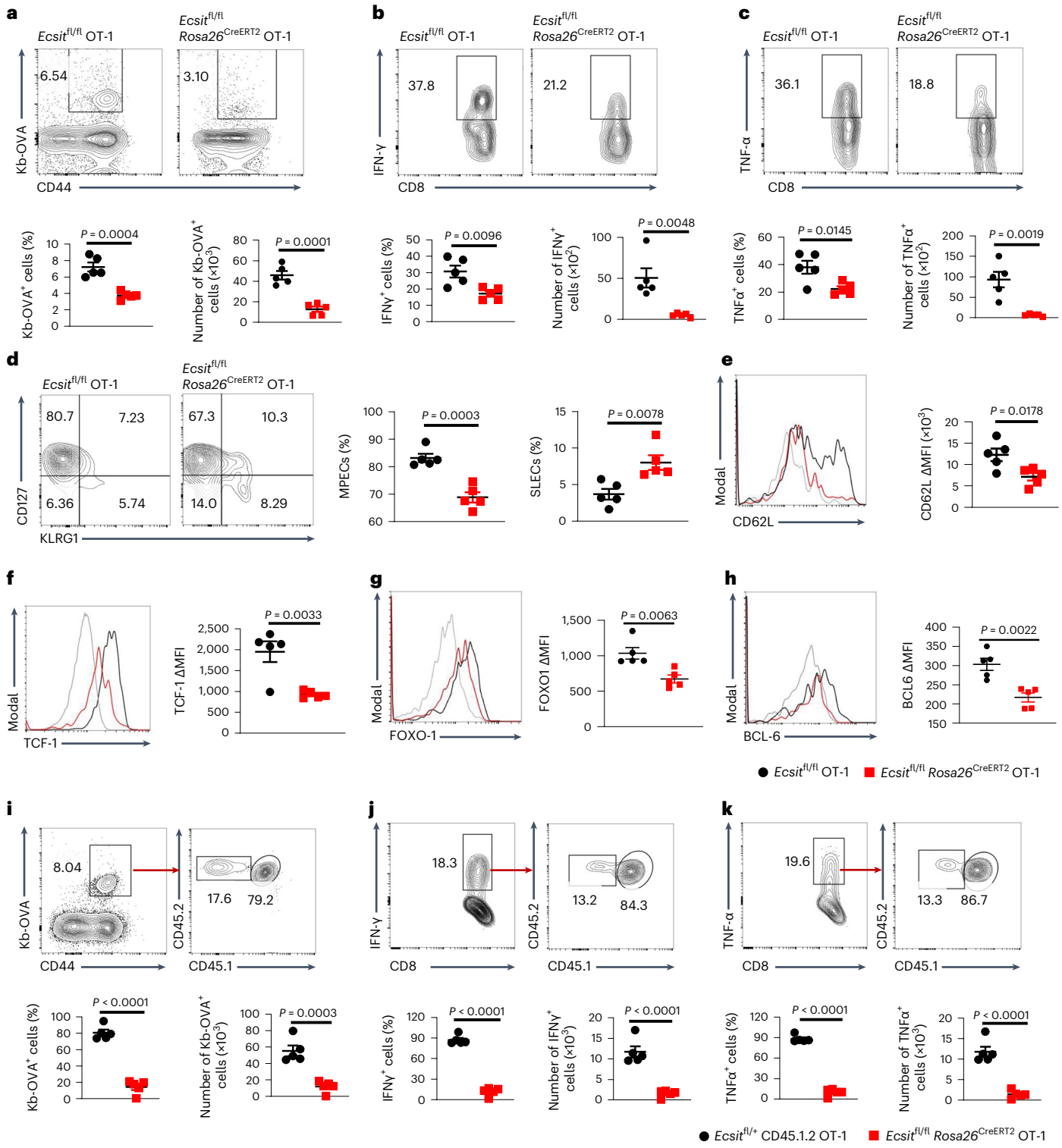

Fig. 2 | ECSIT deficiency impairs memory CD8⁺ T cell differentiation in acute viral infection. a, Representative flow cytometry plots (top) and the percentage and number (bottom) of Kb-OVA⁺CD44⁺CD8⁺ T cells in the spleen. **b**,**c**, Representative flow cytometry plots (top) and the percentage and number (bottom) of IFN-γ⁺ (**b**) and TNF-α⁺ (**c**) subsets of Kb-OVA⁺CD44⁺CD8⁺ T cells in the spleen. **d**, Representative flow cytometry plots (left) and the percentage of MPEC (middle) and SLEC (right) subpopulations of Kb-OVA⁺CD44⁺CD8⁺ T cells in the spleen. **e**–**h**, Flow cytometry analysis of CD62L (**e**), TCF-1 (**f**), FOXO-1 (**g**) and BCL-6 (**h**) expression of Kb-OVA⁺CD44⁺CD8⁺ T cells in the spleen. **i**, Representative flow cytometry plots (top) and the percentage and number (bottom) of *Ecsit*$^{fl/+}$ CD45.1.2 and *Ecsit*$^{fl/fl}$ *Rosa26*^{CreERT2} CD45.2 OT-1 cells in the spleen following gating for Kb-OVA⁺CD44⁺CD8⁺ T cells. **j**,**k**, Representative flow cytometry plots (top) and the percentage and number (bottom) of *Ecsit*$^{fl/+}$ CD45.1.2 and *Ecsit*$^{fl/fl}$ *Rosa26*^{CreERT2} CD45.2 OT-1 cells in the spleen following gating for IFN-γ⁺ (**j**) and TNF-α⁺ (**k**) Kb-OVA⁺CD44⁺CD8⁺ T cells. Data are pooled from three independent experiments; $n = 5$; data are the mean ± s.e.m. Two-tailed unpaired Student's *t*-test.

after ECSIT deletion due to VSV-OVA infection, whereas the expression of the effector-associated transcription factor T-BET[15] was enhanced (Fig. 2f–h and Extended Data Fig. 3h), further suggesting a role for ECSIT in the maintenance of the transcription programme of memory T cells.

To further study the T cell-intrinsic function of ECSIT in the generation of antigen-specific memory CD8$^+$ T cells, we mixed congenically marked OT-1 control *Ecsit*$^{fl/+}$ (CD45.1.2) and *Ecsit*$^{fl/fl}$ *Rosa26*^{CreERT2} (CD45.2) CD8$^+$ T_N cells at a 1:1 ratio and co-transferred them to WT recipient mice (CD45.1), which were then infected with VSV-OVA. Starting on day 21 post infection, the mice were administered five daily doses of tamoxifen to induce ECSIT deletion during memory T cell development (Extended Data Fig. 2k). The percentages of *Ecsit*$^{fl/fl}$ *Rosa26*^{CreERT2} OT-1 cells in the spleen and liver were substantially lower than that the *Ecsit*$^{fl/+}$ OT-1 controls at day 35 post infection (Fig. 2i and Extended Data Fig. 3i). In addition, the majority of IFN-γ- and TNF-α-producing cells in the recipient mice were derived from control, not CD45.2 *Ecsit*$^{fl/fl}$ *Rosa26*^{CreERT2}, OT-1 donor cells (Fig. 2j,k and Extended Data Fig. 3j,k), thus further establishing a cell-intrinsic role for ECSIT in the formation of memory CD8$^+$ T cells during acute viral infection.

ECSIT loss significantly restrains the transcriptional level and regulation of TCF-1, thus blocking memory of CD8$^+$ T cells during acute viral infection

We next performed RNA-sequencing (RNA-seq) analysis of OVA-specific OT-1 memory *Ecsit*$^{fl/+}$ (CD45.1.2; WT) and *Ecsit*$^{fl/fl}$ *Rosa26*^{CreERT2} (CD45.2; induced KO, iKO) CD8$^+$ T cells sorted from the co-transferred CD45.1 WT recipient mice 35 d after VSV-OVA infection (Extended Data Fig. 4a), which revealed a distinct gene cluster (Fig. 3a) and a total of 7,124 differentially expressed genes (DEGs) with a fold change of >1.2 when compared with the controls (Extended Data Fig. 4b). Lymphocyte differentiation, response to virus and metabolic pathways were downregulated in ECSIT-deficient T cells, which showed a significant downregulation in the enrichment of central versus CD8$^+$ T_{EM} cell signatures and *Tcf7* target gene signature compared with WT control cells (Fig. 3b–d). Specially, ECSIT deletion resulted in a decrease in the expression of memory-related receptors (*Sell*, *Ccr7* and *Slamf6*) and transcription factors (*Tcf7*, *Lef1*, *Bcl6* and *Id3*) but elevated expression of genes associated with effector CD8$^+$ T cells (*Cd44*, *Tbx21*, *Stat4*, *Zeb2* and *Id2*; Fig. 3e). Moreover, *Tcf7*, *Fli1*, *Lef1* and *Eomes* were the most enriched transcription factors with DEGs, as determined by transcription factor enrichment analysis using the Chromatin Immunoprecipitation (ChIP)-X Enrichment Analysis version 3 (ChEA3) analysis tool (Fig. 3f).

We next sought to determine the chromatin accessibility profiles of antigen-specific memory CD8$^+$ T cells. Following VSV-OVA infection, WT (CD45.1.2) and iKO (CD45.2) memory CD8$^+$ T cells were isolated for assay for transposase-accessible chromatin using sequencing (ATAC-seq) analysis (Extended Data Fig. 4a,c). The significant downregulation of differentially accessible chromatin regions (DACRs) corresponded to cellular response to viral infection, cell differentiation and metabolic pathway in ECSIT-deficient cells (Extended Data Fig. 4d). Transcription factor motifs of ELF-3, TCF-3, ELF-4 and TCF-1 exhibited upregulation in WT memory CD8$^+$ T cells relative to iKO cells (determined by Hypergeometric Optimization of Motif EnRichment (HOMER) analysis; Fig. 3g). We further identified *Tcf7* as the most enriched transcription factor motif in DACRs responsible for the changes in gene expression (Fig. 3h). The gene loci of important memory-associated genes, such as *Bcl6*, *Lef1*, *Slamf6* and *Ccr7*, were less abundant in overlapped ATAC-seq and TCF-1 peaks in iKO CD8$^+$ T cells relative to WT cells (Fig. 3i and Extended Data Fig. 4e).

To exclude effects due to differences in T_{CM} and T_{EM} subpopulation compositions of WT and iKO cells, we sorted OVA-specific CD8$^+$ T_{CM} and T_{EM} cells and then performed RNA-seq analysis. ECSIT deficiency led to a distinct gene cluster and a significant DEGs in central memory T cells and effector memory T cells between the comparison (fold change > 1.5 and false detection rate < 0.05; Supplementary Fig. 4a,b). Our GSEA analysis of ECSIT-deficient cells revealed significant downregulation of the central memory T cell signature in T_{CM} cells and significant upregulation of the effector memory T cell signature in T_{EM} cells compared with WT controls (Supplementary Fig. 4c). Further analyses (volcano plot and gene heat map) also showed that memory- (*Ccr7*, *Slamf6*, *Tcf7* and *Lef1*) and effector-related genes (*Zeb2*, *Nfatc2* and *Prdm1*) were downregulated and upregulated, respectively, in ECSIT-deficient T_{CM} and T_{EM} cells (Supplementary Fig. 4d,e). Overall, these RNA-seq data further confirm the important role of ECSIT in regulating memory T cell differentiation.

We further assessed the differentiation of WT and iKO memory CD8$^+$ T cells transduced with a retrovirus encoding TCF-1 (TCF-1 overexpression, TCF-1 OE). We analysed the transduced GFP$^+$ cells to detect WT and iKO memory T cell differentiation and found that exogenous TCF-1 expression was significantly higher than that of endogenous TCF-1 (Extended Data Fig. 5a,b). TCF-1 OE promoted the expression of CD62L, CD127, TCF-1 and BCL-6, rescuing memory CD8$^+$ T cell differentiation in iKO cells in vitro (Supplementary Fig. 5a–e). Furthermore, we used a retroviral vector to transduce differentiated OT-1 memory *Ecsit*$^{fl/+}$ (WT CD45.1.2) and *Ecsit*$^{fl/fl}$ *Rosa26*^{CreERT2} (iKO CD45.2) CD8$^+$ T cells with empty vector or TCF-1 (TCF-1 OE) and co-transferred the cells into B6.SJL WT recipient mice (CD45.1), which were then infected with VSV-OVA (Extended Data Fig. 5c). TCF-1 OE also markedly rescued the expansion of ECSIT-deficient OT-1- and IFN-γ-producing CD8$^+$ T cells in the spleen after VSV-OVA infection (Extended Data Fig. 5d,e). Thus, ECSIT promotes memory CD8$^+$ T cell differentiation via TCF-1.

ECSIT deletion reprogrammes metabolism with a significant reduction in fumarate during the differentiation of memory CD8$^+$ T cells

Both RNA-seq and ATAC-seq analyses showed that metabolic pathways were significantly downregulated in ECSIT-deficient T cells. We next performed mass spectrometry (MS)-based metabolomics (Extended Data Fig. 6a). Principal component analysis (PCA) demonstrated clustering of metabolic profiles in two groups. The most significant changes in metabolic pathways in ECSIT-deficient cells were purine, arginine and glutamine metabolism and the tricarboxylic acid cycle (Extended Data Fig. 6b,c). Fumarate was the most downregulated metabolite in ECSIT-deficient cells (Fig. 4a,b and Extended Data Fig. 6d). In line with a decreased oxidative phosphorylation signature detected by RNA-seq (Extended Data Fig. 6e), ECSIT deficiency decreased the oxygen consumption rate (OCR) of memory CD8$^+$ T cells cultured with interleukin (IL)-15 (Extended Data Fig. 6f,g). The OCR decrease was accompanied by an increase in glycolysis (Extended Data Fig. 6h–j). The mitochondria of ECSIT-deficient CD8$^+$ T cells exhibited fragmented cristae (Extended Data Fig. 6k,l). Thus, the loss of ECSIT in CD8$^+$ memory cells impaired cell metabolism with a significant reduction in fumarate, accompanied with defective mitochondria.

Fumarate reduction after ECSIT deficiency leads to impaired CD8$^+$ memory T cell development

H3K4me3 was enriched at the *Tcf7* gene promoter in MPECs and memory CD8$^+$ T cells (Fig. 4c). Fumarate inhibits KDM5 histone demethylases[29]. In agreement with this, the KDM5 activity of ECSIT-deficient memory T cells was significantly higher than the WT controls (Fig. 4d). ECSIT deficiency significantly decreased the level of H3K4me3 modifications and the number of H3K4me3 peaks across the entire genome (Extended Data Fig. 7a,b). *Tcf7* was one of the significant changes among all affected peaks (Fig. 4e). Furthermore, analyses using ChIP with sequencing (ChIP–seq) or quantitative PCR (ChIP–qPCR) confirmed a reduction in H3K4me3 enrichment at the *Tcf7* gene promoter in ECSIT-deficient memory cells (Extended Data Fig. 7c,d). We next reconstituted WT and iKO cells with a cell-permeable form of fumarate (dimethyl fumarate, DMF)[30]. Sorted CD8$^+$ T cells from *Ecsit*$^{fl/fl}$ (WT) and *Ecsit*$^{fl/fl}$ *Rosa26*^{CreERT2} (iKO) OT-1 mice were activated with OVA and IL-2

https://doi.org/10.1038/s41556-024-01351-9

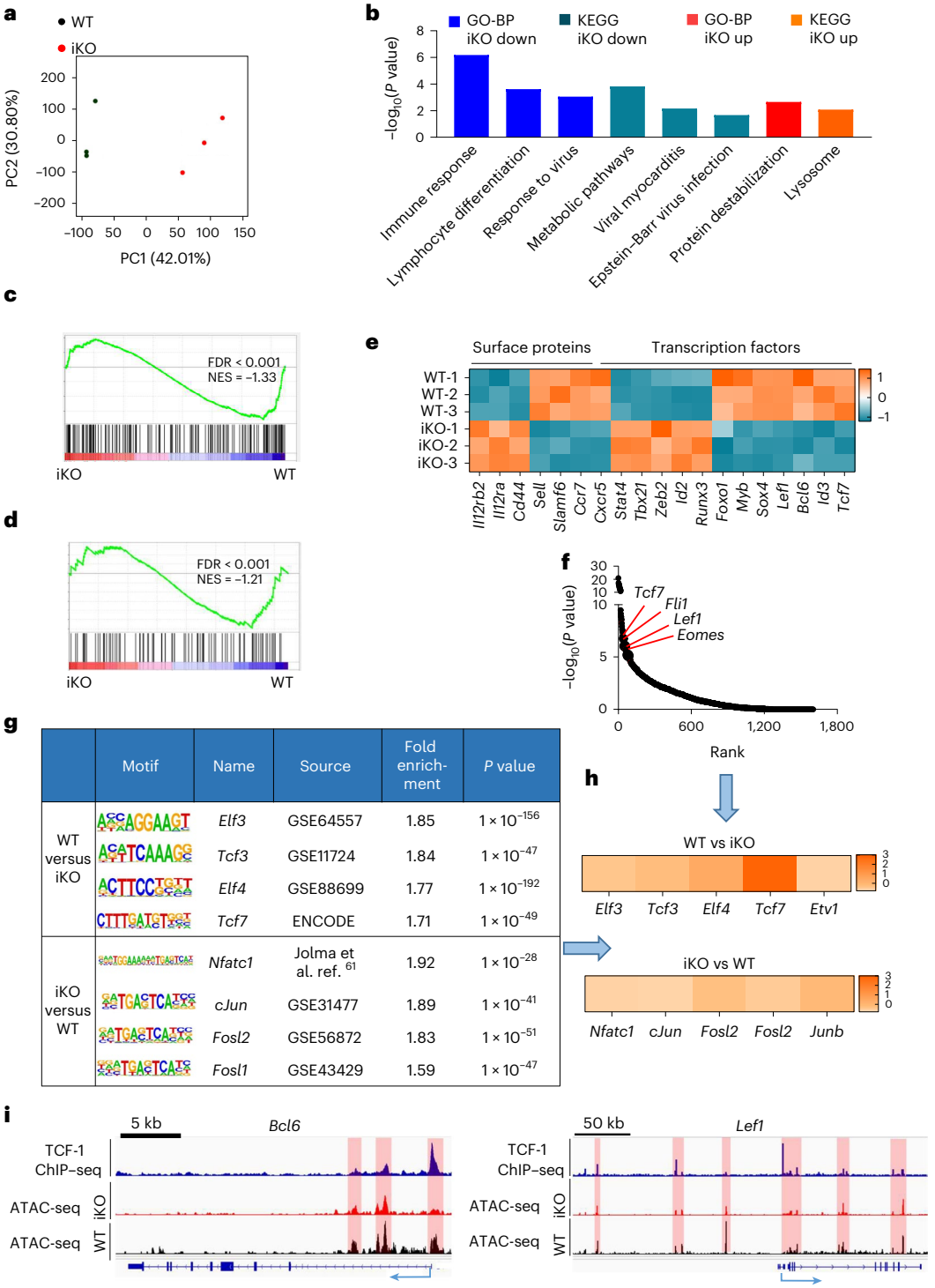

Fig. 3 | ECSIT deficiency impairs memory CD8⁺ T cell differentiation by inhibiting the transcription level and regulation of TCF-1 in acute viral infection. Equal numbers of CD8⁺ T_N cells from *Ecsit*$^{fl/+}$ CD45.1.2 and *Ecsit*$^{fl/fl}$ *Rosa26*^{CreERT2} CD45.2 OT-1 mice were mixed and transferred into CD45.1 recipient mice, which were infected with VSV-OVA 1 d later. The mice were intraperitoneally (i.p.) injected with five doses of tamoxifen (daily injections from day 21 to day 25). OT-1 cells (memory) were sorted on day 35 for RNA-seq and ATAC-seq. **a**, PCA analysis of the RNA-seq data. **b**, Gene ontology biological processes (GO-BP) and Kyoto Encyclopedia of Genes and Genomes (KEGG) analysis of DEGs in *Ecsit*$^{fl/+}$ CD45.1.2 and *Ecsit*$^{fl/fl}$ *Rosa26*^{CreERT2} CD45.2 OT-1 cells. Down, downregulated genes; up, upregulated genes. **c**,**d**, Gene set enrichment analysis (GSEA) of upregulated genes in central CD8⁺ T_M cells compared with effector CD8⁺ T_M cells (GEO accession number GSE23321; **c**) and the top 100 *Tcf7* target genes in GEO accession number GSE164978 (**d**). NES, normalized enrichment score; FDR, false detection rate. **e**, Heat map of surface protein and transcription factor DEGs. The colour bar shows the gene expression (*Z*-score value). **f**, Transcription factor ranks, which are required for DEGs analysed by ChEA3. **g**, HOMER motif analysis of the top transcription factor motifs enriched in DACRs between *Ecsit*$^{fl/+}$ CD45.1.2 and *Ecsit*$^{fl/fl}$ *Rosa26*^{CreERT2} CD45.2 OT-1 cells. **h**, Conjoint analysis of HOMER motif and ChEA3 rank data. The relative rank of the top five transcription factors enriched in *Ecsit*$^{fl/+}$ CD45.1.2 and *Ecsit*$^{fl/fl}$ *Rosa26*^{CreERT2} CD45.2 OT-1 cells in the ChEA3 analysis data. The orange bars show the rank of the transcription factors in **f** (Z-score value). **i**, Genome track view of the *Bcl6* and *Lef1* locus showing ATAC-seq and *Tcf7* ChIP–seq peaks (GEO accession number GSE177064; from T_{CM} cells following acute viral infection). *Tcf7* predictive binding sites (red shadows) are listed. **b**,**f**,**g**, One-sided Fisher's exact test.

https://doi.org/10.1038/s41556-024-01351-9

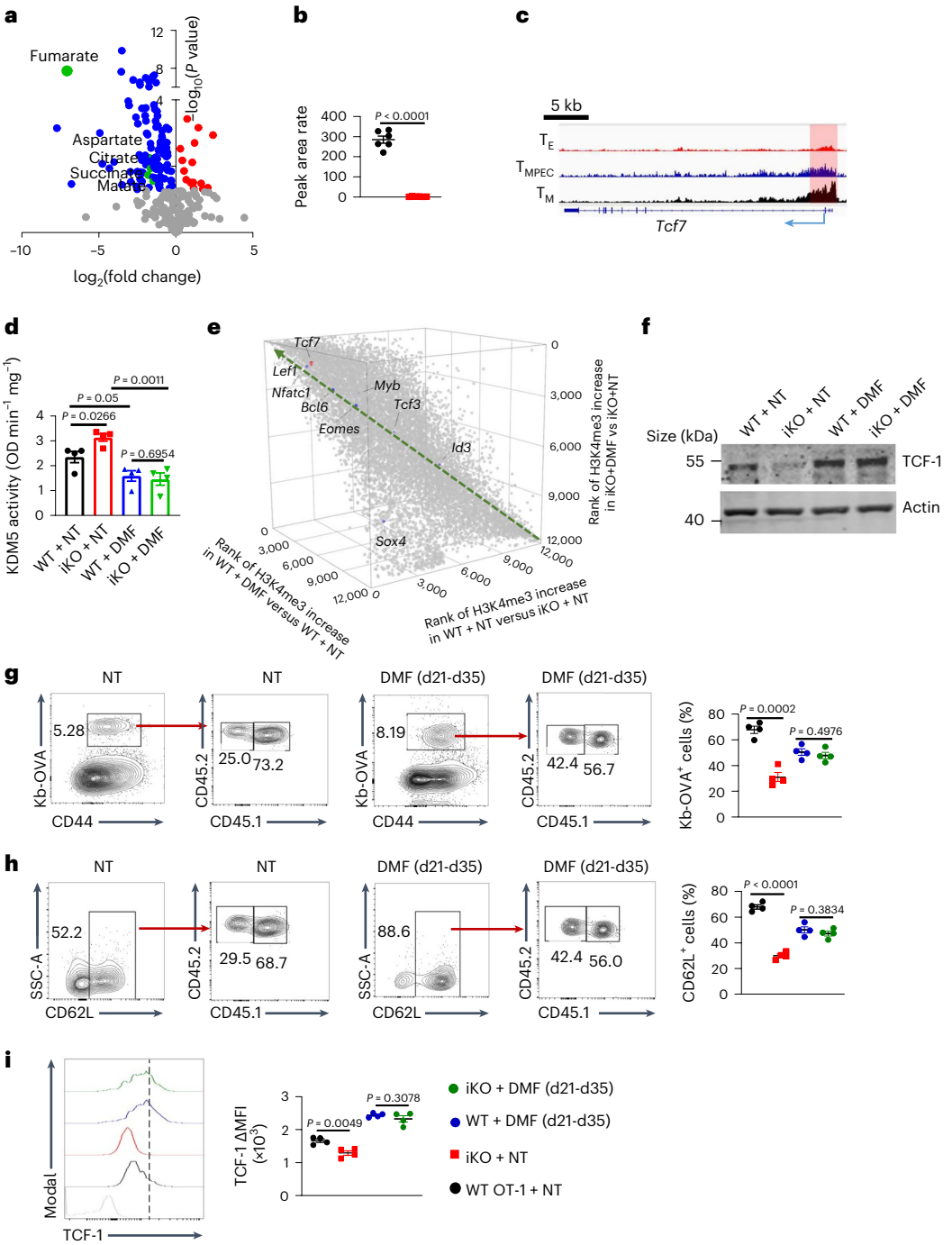

Fig. 4 | ECSIT deficiency inhibits memory CD8⁺ T cell differentiation by reducing fumarate production. a,**b**, Metabolomic analysis of OT-1 *Ecsit*$^{fl/fl}$ (WT) and *Ecsit*$^{fl/fl}$ *Rosa26*^{CreERT2} (iKO) memory CD8⁺ T cells following in vitro IL-15 induction. **a**, Volcano plot of metabolites. **b**, Relative abundance of fumarate. **c**, Genome track view of the *Tcf7* locus showing H3K4me3 peaks in effector T (T_E), MPEC T (T_{MPEC}) and T_M cells in the GEO ChIP–seq dataset GSE95237. **d**, KDM5 activity in WT and iKO memory T cells from an in vitro culture system treated with or without DMF. **e**, Three-dimensional scatter plot showing the ranks of the increase level (based on a Z-statistic) of H3K4me3 from three comparisons: WT + NT versus iKO + NT, WT + DMF versus WT + NT and iKO + DMF versus iKO + NT. *Tcf7* is labelled in red and other memory-related transcription factors are in blue. The dashed green line shows the direction of gene ranking for all three groups. **f**, Immunoblot analysis of TCF-1 expression of memory T cells in the four treatment groups following in vitro induction. **g**,**h**, Representative flow cytometry plots of splenic OT-1 T cells (left; the percentage of cells in the gated regions are indicated) and the percentage (right) of Kb-OVA⁺CD44⁺CD8⁺ (**g**) and CD62L⁺Kb-OVA⁺CD44⁺CD8⁺ subpopulations (**h**). **i**, Flow cytometry analysis of TCF-1 expression gated on CD45.1⁻CD45.2⁺ and CD45.1⁺CD45.2⁺Kb-OVA⁺CD44⁺ CD8⁺ T cells in the spleen. **a**,**b**,**d**,**f**–**i**, Data were pooled from three independent experiments (**d**,**f**–**i**); $n = 6$ (**a**,**b**) or 4 (**d**,**g**–**i**); data are the mean ± s.e.m. The legend in **i** applies to **a**,**b**,**g**–**i**. Two-tailed unpaired Student's *t*-test. NT, no treatment. d21–d35, day 21 to day 35.

for 2 d, after which they were treated with DMF and cultured in the presence of IL-15 and 4-hydroxytamoxifen (4-OHT) for 3 d. The DMF treatment resulted in reduced KDM5 activity and enhanced *Tcf7* promoter H3K4me3 in ECSIT-deleted cells. ChIP–seq analyses revealed that the DMF treatment restored H3K4me3 modifications and H3K4me3 peaks at *Tcf7* in iKO cells to levels comparable to those of WT OT-1 cells

(Fig. 4d and Extended Data Fig. 7a–d). Note that the DMF treatment significantly elevated TCF-1 protein expression in WT and iKO memory T cells (Fig. 4f and Supplementary Fig. 6d). Furthermore, DMF promoted the expression of CD62L, CD127 and BCL-6, restoring the ECSIT-deficient memory CD8$^+$ T cell function (Supplementary Fig. 6a–c,e). Next, we pretreated OT-1 WT (CD45.1.2) and iKO (CD45.2) CD8$^+$ T cells with or without DMF, co-transferred them into B6.SJL WT recipient mice (CD45.1) and then infected the mice with VSV-OVA (Supplementary Fig. 7a). The DMF pretreatment markedly enhanced the expansion of ECSIT-deficient OT-1 IFN-γ-producing CD8$^+$ T cells of the spleen and liver of the recipient mice (Supplementary Fig. 7b–e). To further test the effect of DMF complement on ECSIT-deficient memory T cells in vivo, we co-transferred congenically marked OT-1 *Ecsit*$^{fl/+}$ (WT; CD45.1.2) and *Ecsit*$^{fl/fl}$ *Rosa26*^{CreERT2} (iKO; CD45.2) T_N cells (mixed at a 1:1 ratio) into WT recipient mice (CD45.1) and infected the mice with VSV-OVA. The mice were administered tamoxifen, followed by DMF (Extended Data Fig. 7e). The DMF treatment significantly increased the percentage of CD62L$^+$ and TCF-1$^+$ ECSIT-deficient OT-1 CD8$^+$ T cells compared with the iKO controls (Fig. 4g–i). Thus, ECSIT loss results in the loss of fumarate synthesis and enhanced H3K4me3 demethylation of the *Tcf7* gene, thereby decreasing TCF-1 expression and impairing CD8$^+$ memory T cell formation.

Loss of ECSIT impairs the formation of stem-like memory T cell progenitors and the antitumour function of CD8$^+$ T cells

We next explored the role of ECSIT in mediating the antitumour responses of CD8$^+$ T cells. We sorted congenically marked T_N cells from *Ecsit*$^{fl/fl}$ and *Ecsit*$^{fl/fl}$ *Rosa26*^{CreERT2} OT-1 mice and adoptively transferred them into B6 mice that had been engrafted with B16F10-OVA melanoma cells 24 h previously. The mice were administered tamoxifen to induce ECSIT deletion during the stages of stem-like memory T cell development (Extended Data Fig. 8a). The deletion of ECSIT significantly enhanced tumour progression (Fig. 5a,b). Furthermore, ECSIT deficiency led to a substantial reduction in OVA-specific CD8$^+$ T cells as well as IFN-γ$^+$ and TNF-α$^+$ cells (Fig. 5c–e). ECSIT loss downregulated the $T_{SM\text{-}PEX}$-associated markers SCA-1 and TCF-1 (refs. 9,31) and upregulated TIGIT[32] (Fig. 5f–h). Upregulation of PD-1$^+$TIM-3$^+$ and downregulation of PD-1$^+$TIM-3$^-$ antigen-specific CD8$^+$ T cells was also observed (Fig. 5i). Thus, ECSIT deficiency impairs $T_{SM\text{-}PEX}$ and the antitumour function of CD8$^+$ T cells.

Next, we sought to determine the T cell-intrinsic function of ECSIT in the regulation of the antitumour activity of CD8$^+$ T cells. We mixed congenically marked OT-1 *Ecsit*$^{fl/+}$ (CD45.1.2) and *Ecsit*$^{fl/fl}$ *Rosa26*^{CreERT2} (CD45.2) CD8$^+$ T_N cells at a 1:1 ratio and co-transferred them to WT recipient mice (CD45.1) that had been engrafted with B16F10-OVA melanoma cells. The mice were administered tamoxifen to delete ECSIT (Extended Data Fig. 8b). The percentage of *Ecsit*$^{fl/fl}$ *Rosa26*^{CreERT2} OT-1 cells in the TME was lower than that of the *Ecsit*$^{fl/+}$ OT-1 control cells (Fig. 5j). The majority of IFN-γ- and TNF-α-producing cells were derived from CD45.1.2 control, rather than CD45.2 *Ecsit*$^{fl/fl}$ *Rosa26*^{CreERT2}, OT-1 donor cells (Fig. 5k,l).

ECSIT deficiency restrains the transcriptional expression of TCF-1 and antitumour response of CD8$^+$ T cells by reducing fumarate synthesis

We next isolated OT-1 *Ecsit*$^{fl/+}$ (CD45.1.2; WT) and *Ecsit*$^{fl/fl}$ *Rosa26*^{CreERT2} (CD45.2; iKO) CD8$^+$ T cells from the co-transferred CD45.1 WT recipient mice after engraftment with B16F10-OVA cells and performed RNA-seq analysis (Extended Data Fig. 9a and Fig. 6a). ECSIT deficiency resulted in the downregulation of T cell activation and metabolic pathway as well as a significant decrease in memory CD8$^+$ T cell-related signatures (Fig. 6b–e). Specially, ECSIT deficiency resulted in decreased expression of genes related to exhausted stem-like memory progenitor CD8$^+$ T cells (*Sell*, *Slamf6*, *Tcf7*, *Bcl6*, *Myb* and *Id3*) and elevated expression of genes involved in exhaustion (*Irf4*, *Runx3* and *Nr4a3*; Fig. 6f). Similarly, *Tcf7* was one of most enriched transcription factors associated with DEGs (Fig. 6g).

We next performed ATAC-seq on WT and iKO OT-1 cells. Genes with DACRs—including genes involved in cell differentiation, metabolic pathways and signalling pathways regulating pluripotency of stem cells—were downregulated after ECSIT deficiency (Extended Data Fig. 9b). *Tcf7* was defined as the most significantly targeted transcription factor responsible for the changes in gene expression among the top enrichment of transcription factor motifs in DACRs (Fig. 6h,i). Correspondingly, the gene loci of important genes associated with $T_{SM\text{-}PEX}$ cells—such as *Bcl6*, *Lef1*, *Ccr7* and *Slamf6*—showed lower abundance in overlapped ATAC-seq and TCF-1 peaks in iKO CD8$^+$ T cells relative to the WT cells (Fig. 6j and Extended Data Fig. 9c). Thus, ECSIT promotes the antitumour activity of CD8$^+$ T cells through regulation of TCF-1 expression in the TME. We next used an in vitro OVA continuous stimulation system that can induce $T_{SM\text{-}PEX}$[33] and then analysed WT and iKO OT-1 CD8$^+$ T cells that were retrovirally transduced with TCF-1 (TCF-1 OE; Supplementary Fig. 8a). The expression of SCA-1, BCL-6 and TCF-1 was dramatically promoted by TCF-1 OE in ECSIT-deficient OT-1 cells; however, TIGIT expression was reduced (Supplementary Fig. 8b–g).

We performed MS-based metabolomics analyses of OT-1 WT and iKO CD8$^+$ T cells from an in vitro culture system (Extended Data Fig. 10a–c). Fumarate was significantly reduced in ECSIT-deficient CD8$^+$ T cells (Fig. 7a,b and Extended Data Fig. 10d). We next performed a fumarate rescue assay (Supplementary Fig. 9a). Treatment of iKO cells with DMF significantly reduced KDM5 activity and enhanced *Tcf7* promoter H3K4me3 (Fig. 7c,d). Accordingly, DMF treatment elevated TCF-1 in WT and iKO OT-1 cells (Fig. 7e and Supplementary Fig. 9d) and promoted the expression of SCA-1 and BCL-6, but reduced TIGIT expression, in ECSIT-deficient cells, thus restoring CD8$^+$ T cell function (Supplementary Fig. 9b,c,e). We also pretreated OT-1 WT (CD45.1.2) and iKO (CD45.2) CD8$^+$ T cells with or without DMF in an in vitro culture system and co-transferred them into WT recipient mice (CD45.1) that had been engrafted with B16F10-OVA cells 10 d previously (Supplementary Fig. 10a). Fumarate pretreatment markedly enhanced the expansion of ECSIT-deficient OT-1 CD8$^+$ T cells and their IFN-γ- and CD62L-expressing subsets in the TME (Supplementary Fig. 10b–d). We further mixed congenically marked OT-1 WT (CD45.1.2) and iKO (CD45.2) CD8$^+$ T_N cells at a 1:1 ratio and co-transferred them to WT mice (CD45.1) that had been engrafted with B16F10-OVA cells. The mice were administered tamoxifen and DMF (Extended Data Fig. 10e). The in vivo DMF treatment significantly enhanced the expansion of OT-1 CD62L- and TCF-1-producing ECSIT-deficient CD8$^+$ T cells compared with the iKO controls (Fig. 7f–h).

ECSIT expression correlates positively with stem cell-like memory progenitors of CD8$^+$ T cells, antitumour immunity and the survival of patients with cancer

Additionally, ECSIT expression was significantly higher in $T_{SM\text{-}PEX}$ (CD8-6 and CD8-4 in GEO accession numbers GSE120575 and GSE166181, respectively) than T_{EXH} (CD8-1 in both GSE120575 and GSE166181) cells in the TME of patients with melanoma (Fig. 8a). ECSIT expression correlated negatively with the immune checkpoints HAVCR2, IL-10, CTLA4, TIGIT, CD274 and TGFBR1 in multiple tumour types (Fig. 8b). Moreover, *Ecsit* and $T_{SM\text{-}PEX}$-associated genes—including *Tcf7*, *Bcl6*, *Sell* and *Foxo1*—were highly expressed in patients responding to anti-PD-1 therapy, whereas T_{EXH}-associated genes such as *Pdcd1*, *Ctla4*, *Tigit* and *Tox* were downregulated (Fig. 8c). In addition, ECSIT expression was positively associated with the corresponding prognoses in multiple cancers (Fig. 8d).

Pharmacological administration of fumarate enhances TCF-1 expression and the antitumour immunity of CD8$^+$ T cells during checkpoint blockade

We next treated melanoma-bearing mice with a combination of DMF and anti-PD-L1 (Supplementary Fig. 11a). Treatment with DMF resulted

https://doi.org/10.1038/s41556-024-01351-9

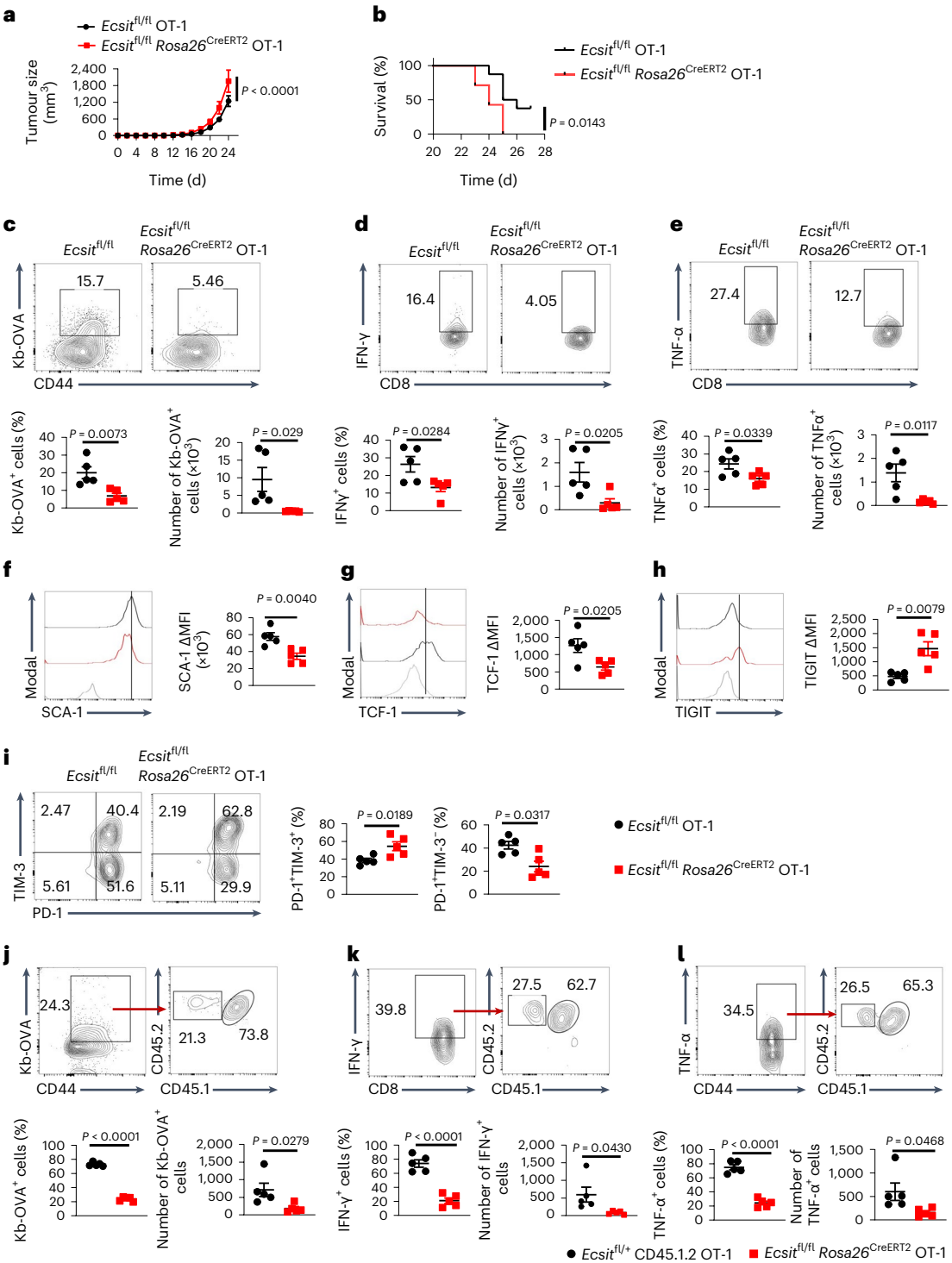

Fig. 5 | ECSIT deficiency impairs the formation of stem cell-like memory T cell progenitors and the antitumour function of CD8⁺ T cells. a, Growth of B16F10-OVA melanomas in *Ecsit*$^{fl/fl}$ and *Ecsit*$^{fl/fl}$ *Rosa26*^{CreERT2} OT-1 mice. **b**, Survival rates of the mice. **c**, Representative flow cytometry plots (top) and the percentage and number (bottom) of Kb-OVA⁺CD44⁺CD8⁺ cells in the TME. **d**,**e**, Representative flow cytometry plots (top) and the percentage and number (bottom) of IFN-γ⁺ (**d**) and TNF-α⁺ (**e**) T cell subsets of Kb-OVA⁺CD44⁺CD8⁺ cells in the TME. **f**–**h**, Flow cytometry analysis of SCA-1 (**f**), TCF-1 (**g**) and TIGIT (**h**) expression in Kb-OVA⁺CD44⁺CD8⁺ cells. **i**, Representative flow cytometry plots (left) and the percentage (right) of PD-1⁺TIM-3⁻ and PD-1⁺TIM-3⁺ cell sunsets of Kb-OVA⁺CD44⁺CD8⁺ cells. **j**, Representative flow cytometry plots of *Ecsit*$^{fl/+}$ CD45.1.2 and *Ecsit*$^{fl/fl}$ *Rosa26*^{CreERT2} CD45.2 OT-1 cells (top) and the percentage and number (bottom) of Kb-OVA⁺CD44⁺CD8⁺ cells in the TME. **k**,**l**, Representative flow cytometry plots (top) and the percentage and number (bottom) of IFN-γ⁺ (**k**) and TNF-α⁺ (**l**) Kb-OVA⁺CD44⁺CD8⁺ T cells derived from *Ecsit*$^{fl/+}$ CD45.1.2 and *Ecsit*$^{fl/fl}$ *Rosa26*^{CreERT2} CD45.2 OT-1 cells. Data were pooled from three independent experiments; $n = 7$ (**a**,**b**) or 5 (**c**–**l**); data are the mean ± s.e.m. Two-way analysis of variance test (**a**), log-rank test (**b**), two-tailed unpaired Student's *t*-test (**c**–**g**,**i**–**l**) and Mann–Whitney two-tailed test (**h**).

https://doi.org/10.1038/s41556-024-01351-9

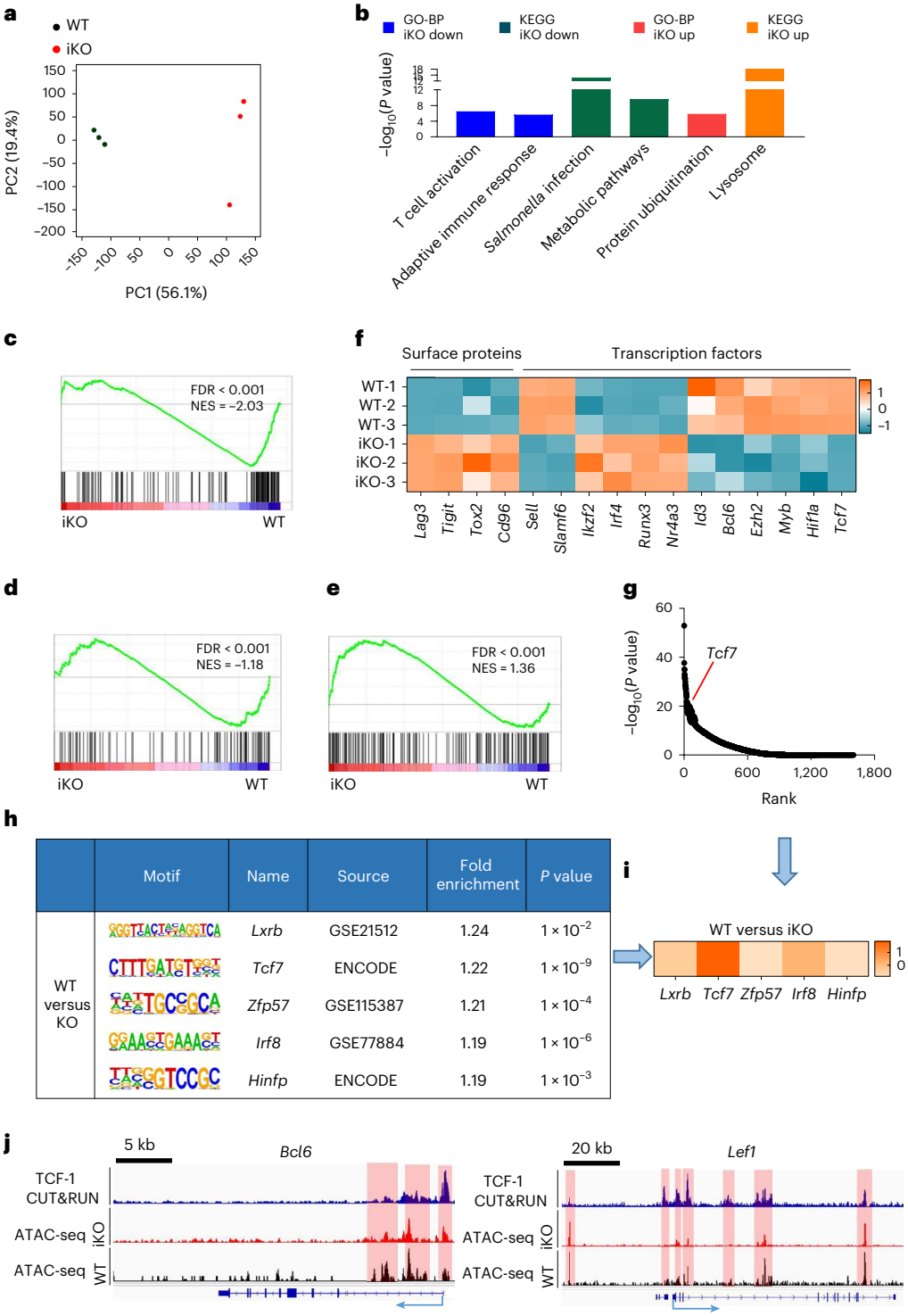

Fig. 6 | ECSIT deficiency impairs the differentiation of stem-like memory CD8$^+$ T cells by inhibiting the transcriptional level and regulation of TCF-1 in chronic tumour stimulation. CD45.1 recipient mice were implanted with B16F10-OVA cells subcutaneously. OT-1 *Ecsit*$^{fl/+}$ CD45.1.2 and *Ecsit*$^{fl/fl}$ *Rosa26*^{CreERT2} CD45.2 CD8$^+$ T_N cells were then mixed and transferred into the mice 1 d later. The recipient mice were treated with five daily doses of tamoxifen through i.p. injection from day 10 to day 15. OT-1 cells were sorted on day 20 for RNA-seq and ATAC-seq. **a**, PCA analysis of the RNA-seq data. **b**, GO and KEGG analysis of DEGs in *Ecsit*$^{fl/+}$ CD45.1.2 and *Ecsit*$^{fl/fl}$ *Rosa26*^{CreERT2} CD45.2 OT-1 cells. **c**–**e**, GSEA analysis of memory signature genes from the GEO GSE23321 dataset (**c**), the top-100 *Tcf7* target genes in GSE164978 (**d**) and upregulated genes in exhausted versus memory CD8$^+$ T cells (GSE9650; **e**). **f**, Heat map of surface protein and transcription factor DEGs. **g**, Transcription factor ranks, which are required for DEGs analysed by ChEA3. **h**, HOMER motif analysis of the top transcription factor motif enriched in DACRs between *Ecsit*$^{fl/+}$ CD45.1.2 and *Ecsit*$^{fl/fl}$ *Rosa26*^{CreERT2} CD45.2 OT-1 cells. **i**, Conjoint analysis of the HOMER motif and ChEA3 rank data. The relative rank of the top five transcription factors enriched in *Ecsit*$^{fl/+}$ CD45.1.2 and *Ecsit*$^{fl/fl}$ *Rosa26*^{CreERT2} CD45.2 OT-1 cells in ChEA3 analysis data. **j**, Genome track view of the *Bcl6* and *Lef1* locus showing ATAC-seq and *Tcf7* CUT&RUN peaks (GEO accession number GSE139056; from CD8$^+$ $T_{EX\text{-}STEM}$ of TME). *Tcf7* predictive binding sites (shaded red regions) are indicated. **b**,**g**,**h**, One-sided Fisher's exact test.

https://doi.org/10.1038/s41556-024-01351-9

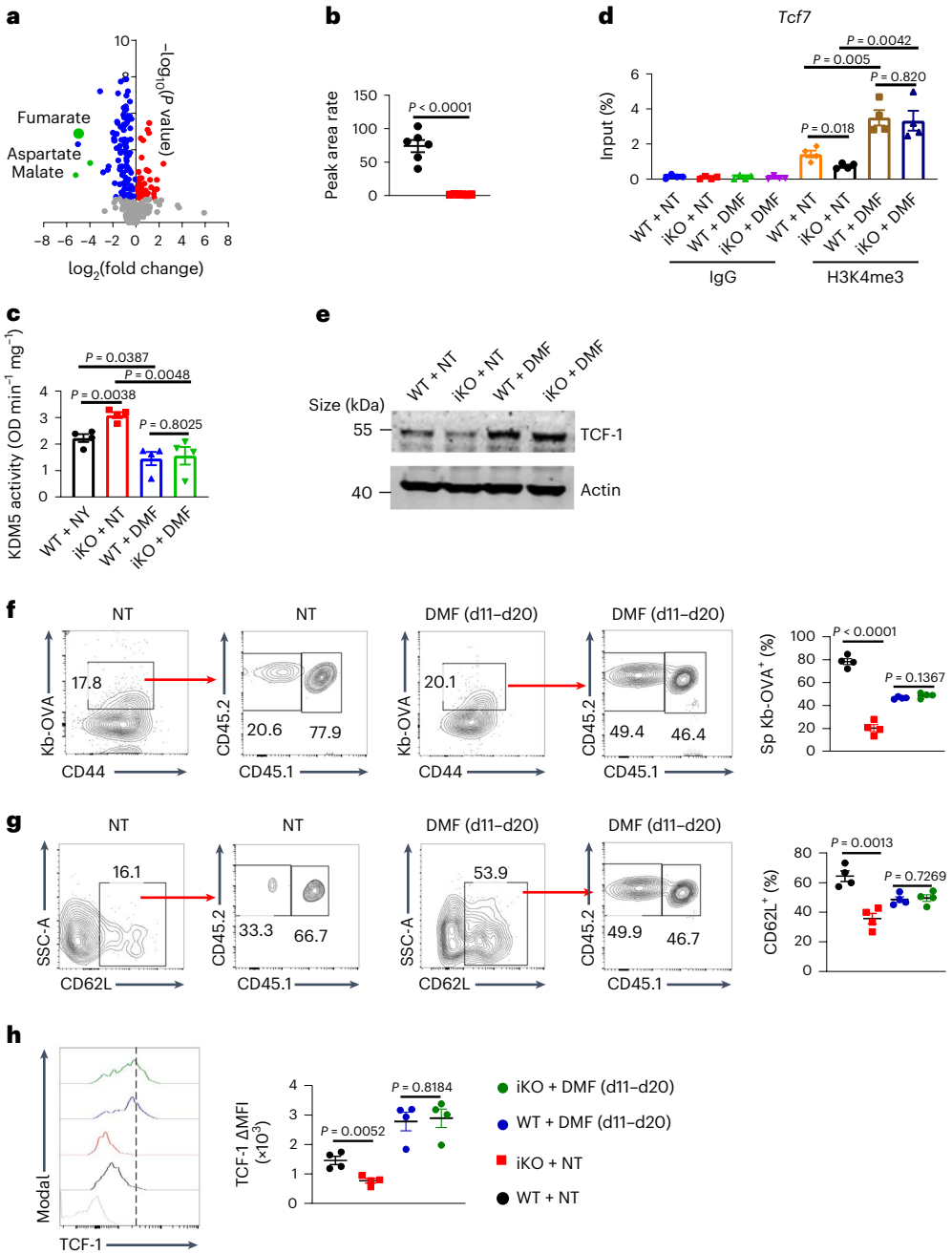

Fig. 7 | ECSIT deficiency inhibits the differentiation of stem cell-like memory CD8⁺ T cells by reducing fumarate production in chronic tumour stimulation. a,**b**, *Ecsit*$^{fl/fl}$ (WT) and *Ecsit*$^{fl/fl}$ *Rosa26*^{CreERT2} (iKO) OT-1 cells were activated with OVA and IL-2 for 2 d, followed by sorting of CD8⁺ T cells. The CD8⁺ T cells were chronically stimulated with IL-15 and OVA for 3 d, to mimic tumour-antigen chronic stimulation, in the presence of 4-OHT. OT-1 cells were collected for metabolomics analysis. **a**, Volcano plot of metabolites. **b**, Relative abundance of fumarate. **c**, KDM5 activity in WT and iKO T cells treated with or without DMF. **d**, ChIP–qPCR analysis of H3K4me3 levels at the promoters of *Tcf7* in T cells of the four treatment groups. **e**, Immunoblot analysis of TCF-1 expression in T cells from the four treatment groups. **f**,**g**, Representative flow cytometry plots of splenic OT-1 T cells (left; the percentage of cells in the gated regions are indicated) and the percentage (right) of Kb-OVA⁺CD44⁺CD8⁺ (**f**) and CD62L⁺Kb-OVA⁺CD44⁺CD8⁺ subpopulations (**g**). **h**, Flow cytometry analysis of TCF-1 expression of CD45.1⁻CD45.2⁺ and CD45.1⁺CD45.2⁺ Kb-OVA⁺CD44⁺CD8⁺ T cells in the tumour. **a**–**h**, Data were pooled from three independent experiments (**c**–**h**); $n = 6$ (**a**,**b**) or 4 (**c**,**d**,**f**–**h**); data are the mean ± s.e.m. The legend in **h** applies to **a**,**b**,**f**–**h**. **a**–**d**,**f**–**h**, Two-tailed unpaired Student's *t*-test. d11–d20, day 11 to day 20.

in reduced tumour burden and increased survival during anti-PD-L1 treatment (Supplementary Fig. 11b,c). Consistent with these data, the abundance of total CD8⁺ T cells as well as IFN-γ- and TNF-α-producing CD8⁺ T cells was increased (Supplementary Fig. 11d–f). In addition, the combined DMF and anti-PD-L1 treatment resulted in significant upregulation in expression of the $T_{SM\text{-}PEX}$-associated marker TCF-1 (Supplementary Fig. 11g).

Discussion

Beyond the function of innate immunity, the roles of ECSIT for other immune cells, especially those in adaptive immunity, remain largely unknown. In this study we found that ECSIT is expressed at high levels in memory CD8⁺ T cells and identified ECSIT as a critical regulator of memory CD8⁺ T cells. Sustained immune protection from CD8⁺ T cells relies heavily on the generation of memory CD8⁺ T cells to regenerate

https://doi.org/10.1038/s41556-024-01351-9

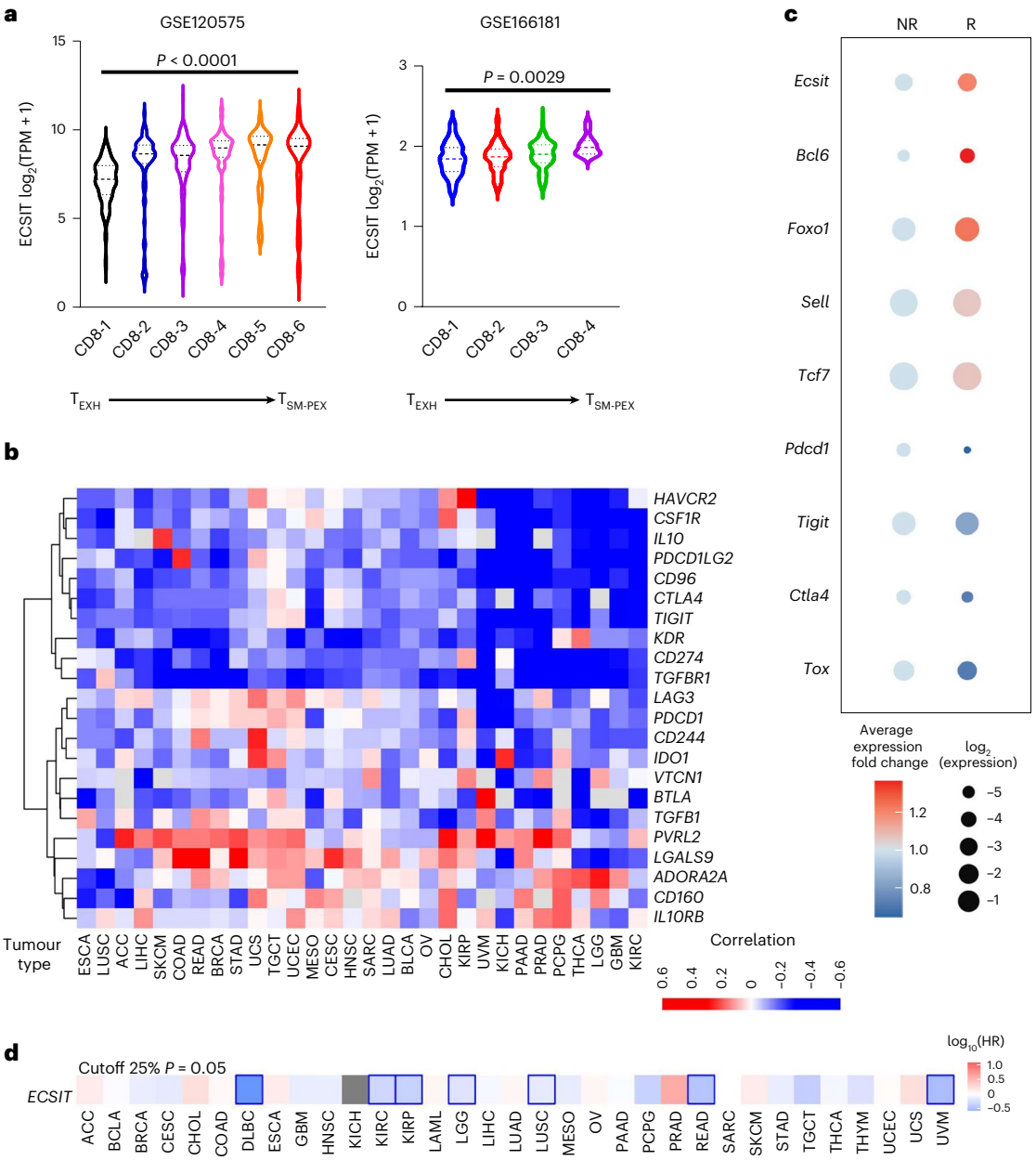

Fig. 8 | ECSIT expression is positively correlated with stem cell-like memory progenitors of CD8⁺ T cells, antitumour immunity and the survival of patients with cancer. a, *ECSIT* expression in CD8⁺ $T_{SM\text{-}PEX}$ cells and terminally exhausted CD8⁺ T cells (T_{EXH}). TPM, transcripts per million. The dashed lines show the quartiles and the median. **b**, Correlation analysis of gene expression profiles between *ECSIT* and immune-checkpoint genes from the TISIDB web portal (http://cis.hku.hk/TISIDB/index.php). **c**, Bubble plot showing the indicated gene expression levels in patients with melanoma who respond (R) or not (NR) to anti-PD-1 therapy (GEO accession number GSE166181). **d**, Survival map of *ECSIT* from pan-cancer using the Gene Expression Profiling Interactive Analysis 2 platform. *ECSIT* expression from The Cancer Genome Atlas data was scored; the top 25% and lowest 25% were considered as high and low expression (cutoff of 25%), respectively. HR, Hazard's ratio. **a**,**d**, Two-tailed unpaired Student's *t*-test (**a**) and log-rank test (**d**). **b**,**d**, Abbreviations are according to the database.

effectors during recurrent antigen exposure[34]. The TCF-1-centred transcriptional network plays a master role in the generation of memory CD8⁺ T cells including long-lived memory[11,18]. However, there have been no in-depth studies on the crucial factors involved in regulating TCF-1 expression and activity. Here we found that ECSIT loss in CD8⁺ T cells led to metabolic changes with a significant reduction in fumarate, resulting in the H3K4me3 demethylation of the TCF-1 promoter region by the histone demethylase KDM5. Perturbed TCF-1 expression in ECSIT-deficient cells impaired the generation and function of memory CD8⁺ T cells in acute viral infection or chronic tumour antigen stimulation.

ECSIT deficiency can lead to marked mitochondrial dysfunction in memory CD8⁺ T cells, including a decreased OCR and fragmented mitochondrial shape (Extended Data Fig. 6e–g,k,l). However, a variety of pathways are known to regulate fumarate production[35–40], including succinate dehydrogenase and fumarate hydratase localization in mitochondria[41], and other enzymes that mainly function in the cytoplasm[42–45]. A number of studies have ascribed additional functions for ECSIT in innate immune signalling in the cytoplasm. Thus, the exact mechanism by which ECSIT regulates the synthesis of fumarate by targeting the mitochondrial or cytoplasmic synthesis enzymes will be of future interest.

The *Tcf7* gene promoter was enriched for H3K4me3 modifications in MPECs and memory CD8$^+$ T cells (Fig. 4c), suggesting that the expression of *Tcf7* might be tightly regulated by KDM-mediated H3K4me3 demethylation in the development of memory cells. Fumarate acts as a competitive inhibitor of histone lysine demethylases (KDMs)[29]. Fumarate supplementation by DMF indeed restored TCF-1 expression and CD8$^+$ T cell function in ECSIT-deficient cells (Figs. 4f–i and 7e–h). Although fumarate also affects histone H3 lysine 27 acetylation modifications and *Tcf7* gene expression can be regulated by histone H3 lysine 27 acetylation modifications[46], these do not conflict with our main finding: ECSIT can regulate the production of fumarate to control KDM5 activity, thereby promoting H3K4me3 modification and expression of the *Tcf7* gene as well as the formation of memory CD8$^+$ T cells[47]. However, the role of fumarate in the progression of CD8$^+$ T cells is complex. Some studies have suggested that fumarate also can suppress effector CD8$^+$ T cells and is used to inhibit CD8$^+$ T effector cells in patients with multiple sclerosis[30,48]. Notably, studies from our laboratory and others have shown that DMF treatment or knockout of the DMF target GSDMD can enhance the expression of PD-1/PD-L1 on CD8$^+$ T or tumour cells, respectively[49,50]. Accordingly, we highlight the potential antitumour therapeutic value of developing strategies to combine DMF with anti-PD-L1 therapy. This is supported by our results demonstrating that DMF with anti-PD-L1 therapy resulted in reduced tumour burden, increased survival and increased abundance of TCF-1$^+$ and cytotoxic CD8$^+$ T cells in melanoma-bearing mice (Supplementary Fig. 11). In addition, our recent study has suggested that DMF can inhibit GSDMD-mediated pyroptosis in innate immune cells to enhance cGAS-induced IFN-stimulated genes, thus promoting antitumour immunity in combination with anti-PD-L1 therapy[50]. Therefore, we have further expanded the therapeutic utility of DMF function.

In summary, our study describes the ECSIT–fumarate–TCF-1 signalling pathway as an essential mediator of CD8$^+$ memory T cell development and provides a molecular framework that defines the importance of ECSIT in regulating antiviral and antitumour responses.

Online content

Any methods, additional references, Nature Portfolio reporting summaries, source data, extended data, supplementary information, acknowledgements, peer review information; details of author contributions and competing interests; and statements of data and code availability are available at https://doi.org/10.1038/s41556-024-01351-9.

References

1. Kaech, S. M. & Ahmed, R. Memory CD8$^+$ T cell differentiation: initial antigen encounter triggers a developmental program in naive cells. *Nat. Immunol.* **2**, 415–422 (2001).
2. Jameson, S. C. & Masopust, D. Diversity in T cell memory: an embarrassment of riches. *Immunity* **31**, 859–871 (2009).
3. Chen, Y., Zander, R., Khatun, A., Schauder, D. M. & Cui, W. Transcriptional and epigenetic regulation of effector and memory CD8 T cell differentiation. *Front. Immunol.* **9**, 2826 (2018).
4. McLane, L. M., Abdel-Hakeem, M. S. & Wherry, E. J. CD8 T cell exhaustion during chronic viral infection and cancer. *Annu. Rev. Immunol.* **37**, 457–495 (2019).
5. Joshi, N. S. et al. Inflammation directs memory precursor and short-lived effector CD8$^+$ T cell fates via the graded expression of T-bet transcription factor. *Immunity* **27**, 281–295 (2007).
6. Martin, M. D. & Badovinac, V. P. Defining memory CD8 T cell. *Front. Immunol.* **9**, 2692 (2018).
7. Hashimoto, M. et al. CD8 T cell exhaustion in chronic infection and cancer: opportunities for interventions. *Annu. Rev. Med.* **69**, 301–318 (2018).
8. Reading, J. L. et al. The function and dysfunction of memory CD8$^+$ T cells in tumor immunity. *Immunol. Rev.* **283**, 194–212 (2018).
9. Siddiqui, I. et al. Intratumoral Tcf1$^+$ PD-1$^+$ CD8$^+$ T cells with stem-like properties promote tumor control in response to vaccination and checkpoint blockade immunotherapy. *Immunity* **50**, 195–211 (2019).
10. Gattinoni, L., Speiser, D. E., Lichterfeld, M. & Bonini, C. T memory stem cells in health and disease. *Nat. Med.* **23**, 18–27 (2017).
11. Zhou, X. et al. Differentiation and persistence of memory CD8$^+$ T cells depend on T cell factor 1. *Immunity* **33**, 229–240 (2010).
12. Ichii, H. et al. Role for Bcl-6 in the generation and maintenance of memory CD8$^+$ T cells. *Nat. Immunol.* **3**, 558–563 (2002).
13. Yang, C. Y. et al. The transcriptional regulators Id2 and Id3 control the formation of distinct memory CD8$^+$ T cell subsets. *Nat. Immunol.* **12**, 1221–1229 (2011).
14. Rutishauser, R. L. et al. Transcriptional repressor Blimp-1 promotes CD8$^+$ T cell terminal differentiation and represses the acquisition of central memory T cell properties. *Immunity* **31**, 296–308 (2009).
15. Xin, A. et al. A molecular threshold for effector CD8$^+$ T cell differentiation controlled by transcription factors Blimp-1 and T-bet. *Nat. Immunol.* **17**, 422–432 (2016).
16. Chen, J. et al. NR4A transcription factors limit CAR T cell function in solid tumours. *Nature* **567**, 530–534 (2019).
17. Khan, O. et al. TOX transcriptionally and epigenetically programs CD8$^+$ T cell exhaustion. *Nature* **571**, 211–218 (2019).
18. Escobar, G., Mangani, D. & Anderson, A. C. T cell factor 1: a master regulator of the T cell response in disease. *Sci. Immunol.* **5**, eabb9726 (2020).
19. Xiao, C. et al. Ecsit is required for Bmp signaling and mesoderm formation during mouse embryogenesis. *Genes Dev.* **17**, 2933–2949 (2003).
20. Wi, S. M. et al. TAK1–ECSIT–TRAF6 complex plays a key role in the TLR4 signal to activate NF-κB. *J. Biol. Chem.* **289**, 35205–35214 (2014).
21. Wen, H. et al. Recurrent ECSIT mutation encoding V140A triggers hyperinflammation and promotes hemophagocytic syndrome in extranodal NK/T cell lymphoma. *Nat. Med.* **24**, 154–164 (2018).
22. West, A. P. et al. TLR signalling augments macrophage bactericidal activity through mitochondrial ROS. *Nature* **472**, 476–480 (2011).
23. Carneiro, F. R., Lepelley, A., Seeley, J. J., Hayden, M. S. & Ghosh, S. An essential role for ECSIT in mitochondrial complex I assembly and mitophagy in macrophages. *Cell Rep.* **22**, 2654–2666 (2018).
24. Xu, L. et al. ECSIT is a critical limiting factor for cardiac function. *JCI Insight* **6**, e142801 (2021).
25. Yang, S. et al. ECSIT is a critical factor for controlling intestinal homeostasis and tumorigenesis through regulating the translation of YAP protein. *Adv. Sci.* **10**, e2205180 (2023).
26. Zhang, N. & Bevan, M. J. TGF-β signaling to T cells inhibits autoimmunity during lymphopenia-driven proliferation. *Nat. Immunol.* **13**, 667–673 (2012).
27. Hogquist, K. A. et al. T cell receptor antagonist peptides induce positive selection. *Cell* **76**, 17–27 (1994).
28. Delpoux, A., Lai, C.-Y., Hedrick, S. M. & Doedens, A. L. FOXO1 opposition of CD8$^+$ T cell effector programming confers early memory properties and phenotypic diversity. *Proc. Natl Acad. Sci. USA* **114**, E8865–E8874 (2017).
29. Arts, R. J. et al. Glutaminolysis and fumarate accumulation integrate immunometabolic and epigenetic programs in trained immunity. *Cell Metab.* **24**, 807–819 (2016).
30. Kornberg, M. D. et al. Dimethyl fumarate targets GAPDH and aerobic glycolysis to modulate immunity. *Science* **360**, 449–453 (2018).
31. Gattinoni, L. et al. A human memory T cell subset with stem cell-like properties. *Nat. Med.* **17**, 1290–1297 (2011).

32. Thommen, D. S. & Schumacher, T. N. T cell dysfunction in cancer. *Cancer Cell* **33**, 547–562 (2018).
33. Zhu, L. et al. Dapl1 controls NFATc2 activation to regulate CD8$^+$ T cell exhaustion and responses in chronic infection and cancer. *Nat. Cell Biol.* **24**, 1165–1176 (2022).
34. Kaech, S. M. & Cui, W. Transcriptional control of effector and memory CD8$^+$ T cell differentiation. *Nat. Rev. Immunol.* **12**, 749–761 (2012).
35. Ryan, D. G. et al. Coupling Krebs cycle metabolites to signalling in immunity and cancer. *Nat. Metab.* **1**, 16–33 (2019).
36. Levicán, G., Ugalde, J. A., Ehrenfeld, N., Maass, A. & Parada, P. Comparative genomic analysis of carbon and nitrogen assimilation mechanisms in three indigenous bioleaching bacteria: predictions and validations. *BMC Genomics* **9**, 581 (2008).
37. de Castro Fonseca, M., Aguiar, C. J., da Rocha Franco, J. A., Gingold, R. N. & Leite, M. F. GPR91: expanding the frontiers of Krebs cycle intermediates. *Cell Commun. Signal.* **14**, 3 (2016).
38. Keshet, R., Szlosarek, P., Carracedo, A. & Erez, A. Rewiring urea cycle metabolism in cancer to support anabolism. *Nat. Rev. Cancer* **18**, 634–645 (2018).
39. Nguyen, B. D. et al. Import of aspartate and malate by DcuABC drives H2/fumarate respiration to promote initial *Salmonella* gut-lumen colonization in mice. *Cell Host Microbe* **27**, 922–936 (2020).
40. Kaufman, S. A model of human phenylalanine metabolism in normal subjects and in phenylketonuric patients. *Proc. Natl Acad. Sci. USA* **96**, 3160–3164 (1999).
41. King, A., Selak, M. & Gottlieb, E. Succinate dehydrogenase and fumarate hydratase: linking mitochondrial dysfunction and cancer. *Oncogene* **25**, 4675–4682 (2006).
42. Cohen, N. S. & Kuda, A. Argininosuccinate synthetase and argininosuccinate lyase are localized around mitochondria: an immunocytochemical study. *J. Cell. Biochem.* **60**, 334–340 (1996).
43. Bergeron, A., D'Astous, M., Timm, D. E. & Tanguay, R. M. Structural and functional analysis of missense mutations in fumarylacetoacetate hydrolase, the gene deficient in hereditary tyrosinemia type 1. *J. Biol. Chem.* **276**, 15225–15231 (2001).
44. Taha-Mehlitz, S. et al. Adenylosuccinate lyase is oncogenic in colorectal cancer by causing mitochondrial dysfunction and independent activation of NRF2 and mTOR-MYC-axis. *Theranostics* **11**, 4011–4029 (2021).
45. Shcherbakova, V., Fechina, V. & Iakovleva, V. Isolation of spheroplasts from *Escherichia coli* 85 for aspartate-ammonia-lyase localization (in Russian). *Prikladnaia Biokhimiia i Mikrobiologiia* **24**, 400–404 (1988).
46. He, B. et al. CD8$^+$ T cells utilize highly dynamic enhancer repertoires and regulatory circuitry in response to infections. *Immunity* **45**, 1341–1354 (2016).
47. Zhai, X. et al. Mitochondrial C1qbp promotes differentiation of effector CD8$^+$ T cells via metabolic-epigenetic reprogramming. *Sci. Adv.* **7**, eabk0490 (2021).
48. Spencer, C. M., Crabtree-Hartman, E. C., Lehmann-Horn, K., Cree, B. A. & Zamvil, S. S. Reduction of CD8$^+$ T lymphocytes in multiple sclerosis patients treated with dimethyl fumarate. *Neurol. Neuroimmunol. Neuroinflammation* **2**, e76 (2015).
49. Garcia, J. et al. Progressive multifocal leukoencephalopathy on dimethyl fumarate with preserved lymphocyte count but deep T-cells exhaustion. *Mult. Scler.* **27**, 640–644 (2021).
50. Jiang, Y. et al. Gasdermin D restricts anti-tumor immunity during PD-L1 checkpoint blockade. *Cell Rep.* **41**, 111553 (2022).

Methods

The research conducted in this study complies with all of the relevant ethical regulations. All experiments were performed with age-matched male mice. All mice were kept in a barrier facility and all animal experiments were conducted in accordance with the procedure approved by the Ethical Review Committee for Laboratory Animal Welfare of Nanjing Medical University (approval number IACUC-1811006-3) and the Nanjing University of Chinese Medicine (approval number 202006A010).

Mice

All mice had a C57BL/6 genetic background except for the CD45.1 mice (B6.SJL strain). *Ecsit*$^{fl/fl}$ mice were generated by clustered regularly interspaced short palindromic repeats (CRISPR)–CRISPR associated protein 9 (Cas9) genome engineering by Biocytogen. Two single guide RNAs were designed using the CRISPR design tool (http://crispr.mit.edu) to target a region either upstream or downstream of exon 4 of *Ecsit* and then screened for on-target activity using a Universal CRISPR activity assay. *Ecsit*–EGFP was generated by CRISPR–Cas9-mediated genome engineering by Cyagen Biosciences. The single guide RNA targeting the mouse *Ecsit* gene, the donor vector containing the '3×Flag-2A-EGFP' cassette and Cas9 messenger RNA were co-injected into fertilized mouse eggs to generate targeted conditional knock-in offspring. F_0 founder animals were identified by PCR, followed by sequence analysis and bred with WT mice to test for germline transmission and F_1 animal generation.

To obtain mature T cell-conditional *Ecsit*-knockout mice, *Ecsit*$^{fl/fl}$ mice were crossed with *dLck*-Cre mice (a gift from L. Lu, Zhejiang University, China). *Ecsit*-floxed mice were also crossed with *Rosa26*^{CreERT2} mice (a gift from X. Zhang, Huazhong University of Science and Technology, China) to generate tamoxifen-induced *Ecsit*-knockout mice (*Ecsit*$^{fl/fl}$ *Rosa26*^{CreERT2}). *Ecsit*$^{fl/fl}$, *Ecsit*$^{fl/fl}$ *dLck*-Cre and *Ecsit*$^{fl/fl}$ *Rosa26*^{CreERT2} mice were crossed with OT-1 mice (a gift from H. Wang, ShanghaiTech University, China) to generate *Ecsit*$^{fl/fl}$, *Ecsit*$^{fl/fl}$ *dLck*-Cre and *Ecsit*$^{fl/fl}$ *Rosa26*^{CreERT2} mice that responded to $OVA_{257–264}$ (*Ecsit*$^{fl/fl}$ OT-1, *Ecsit*$^{fl/fl}$ *dLck*-Cre OT-1 and *Ecsit*$^{fl/fl}$ *Rosa26*^{CreERT2} OT-1). The *Ecsit*$^{fl/fl}$ OT-1 mice were crossed with CD45.1 mice (a gift from X. Wang, Nanjing Medical University, China) to obtain *Ecsit*$^{fl/+}$ CD45.1.2 OT-1 mice. *Rag1*$^{-/-}$ (a gift from Y. Xiao, Shanghai Institute of Nutrition and Health, University of Chinese Academy of Sciences, China).

Cell lines

B16F10 and B16F10-OVA (a gift from C. Xu, Institute of Biochemistry and Cell Biology, Chinese Academy of Sciences, China) cells were maintained at 37 °C with 5% CO_2 in RPMI 1640 medium supplemented with 10% heat-inactivated fetal calf serum and 1% penicillin and streptomycin. Plat-E cells (a gift from X. Wang, Nanjing Medical University, China) were maintained at 37 °C with 5% CO_2 in DMEM medium supplemented with 10% heat-inactivated fetal calf serum and 1% penicillin and streptomycin.

Bone marrow chimaeras

Rag1$^{-/-}$ recipient mice were subjected to lethal-dose irradiation (5 Gy). One day later bone marrow cells from *Ecsit*$^{fl/fl}$ or *Ecsit*$^{fl/fl}$ *dLck*-Cre donor mice were mixed with equal numbers of bone marrow cells from CD45.1 donor mice and 1×10^7 of these mixed cells were intravenously (i.v.) injected into the *Rag1*$^{-/-}$ recipient mice. Chimaeras were analysed 8 weeks after transplantation

Acute and chronic stimulation in vitro of T cells

Splenocytes from OT-1 mice were stimulated with recombinant murine IL-2 (10 ng ml^{-1}; PeproTech) and OVA peptide (1 μg ml^{-1}) in RPMI 1640 medium (supplemented with 10% heat-inactivated fetal calf serum, 2 mM L-glutamine, 1 mM sodium pyruvate, 10 mM HEPES, 5 μM β-mercaptoethanol and 1% penicillin and streptomycin for 2 d). CD8$^+$ T cells were then purified (>95% purity) by negative selection using an EasySep mouse CD8$^+$ T cell isolation kit (Stem Cell Technologies, 19853).

To induce memory T cell differentiation in vitro, purified CD8$^+$ T cells were stimulated with recombinant murine IL-15 (10 ng ml^{-1}; PeproTech) for 3 d. Both 4-OHT (300 nM) and DMF (30 μM) were added to the culture medium to delete *Ecsit* and supplement fumarate, respectively, in CD8$^+$ T cells of *Ecsit*$^{fl/fl}$ *Rosa26*^{CreERT2} OT-1 mice.

To mimic tumour-antigen chronic stimulation in vitro, purified CD8$^+$ T cells were subjected to daily repeated stimulations with OVA peptide (1 μg ml^{-1}) in the presence of recombinant murine IL-15 (10 ng ml^{-1}; PeproTech) for 3 d. Both 4-OHT (300 nM) and DMF (30 μM) were added to the culture medium to delete *Ecsit* and supplement fumarate, respectively, in CD8$^+$ T cells of *Ecsit*$^{fl/fl}$ *Rosa26*^{CreERT2} OT-1 mice.

Acute infection

To analyse effector T cells, 5×10^4 naive *Ecsit*$^{fl/fl}$ or *Ecsit*$^{fl/fl}$ *dLck*-Cre OT-1 cells were i.v. transferred into WT recipient mice. The recipient mice were i.v. injected 1 d later with 1×10^5 plaque-forming units of VSV-OVA; the mice were killed for FACS analysis on day 7.

To analyse recall responses, 5×10^4 naive *Ecsit*$^{fl/fl}$ or *Ecsit*$^{fl/fl}$ *dLck*-Cre OT-1 cells were i.v. transferred into WT recipient mice. The recipient mice were i.v. injected 1 d later with 1×10^5 plaque-forming units of VSV-OVA. CD8$^+$CD44$^+$Kb-OVA$^+$ cells were sorted on day 35 and then adoptively transferred into naive WT recipient mice (1×10^4 cells per mouse), followed by i.v. injection with 5×10^4 colony-forming units of LM-OVA. The recall response was analysed on day 5 after the second infection.

For WT recipient mice, 5×10^4 naive *Ecsit*$^{fl/fl}$ or *Ecsit*$^{fl/fl}$ *Rosa26*^{CreERT2} OT-1 cells were i.v. transferred into recipient mice. The recipient mice were i.v. injected 1 d later with 1×10^5 plaque-forming units of VSV-OVA. The recipient mice were i.p. injected with tamoxifen on days 21–25 and were killed for FACS analysis on day 35.

For CD45.1 recipient mice, 4×10^4 naive *Ecsit*$^{fl/+}$ CD45.1.2 OT-1 cells were mixed with equal numbers of naive *Ecsit*$^{fl/fl}$ *Rosa26*^{CreERT2} CD45.2 OT-1 cells and then i.v. transferred into CD45.1 recipient mice. The recipient mice were i.v. injected with 1×10^5 plaque-forming units of VSV-OVA 1 d later. The recipient mice were treated with tamoxifen via i.p. injection from day 21 to day 25 and killed for FACS analysis on day 35. In some experiments, the recipient mice were treated with DMF at a dose of 10 mg kg^{-1} every other day from day 21 to day 35. For the in vivo TCF-1 OE experiments, 4×10^5 *Ecsit*$^{fl/+}$ (CD45.1.2) and *Ecsit*$^{fl/fl}$ *Rosa26*^{CreERT2} (CD45.2) OT-1 CD8$^+$ memory T cells were retrovirally transduced with empty vector or TCF-1 (TCF-1 OE). Next, WT and iKO (GFP$^+$FVD$^-$) CD8$^+$ T cells were sorted and co-transferred into B6.SJL WT recipient mice (CD45.1), followed by infection with 1×10^5 plaque-forming units of VSV-OVA. The recipient mice were killed on day 5 for FACS analysis.

Tumour models

Age- and sex-matched recipient mice were anaesthetized with 1.2% (wt/vol) tribromoethanol (20 μl g^{-1} mouse weight) by i.p. injection. The mice were then subcutaneously injected on the flank with 1×10^5 B16F10 or B16F10-OVA cells in 100 μl PBS. For WT recipient mice, the mice were i.v. administered 2×10^5 *Ecsit*$^{fl/fl}$ or *Ecsit*$^{fl/fl}$ *Rosa26*^{CreERT2} naive OT-1 cells 1 d after implantation. The tumour size (determined by caliper measurements and calculated as length × width × width / 2) was recorded every 2 d from day 10. The mice were euthanized when the tumour size exceeded 1,500 mm^3. For CD45.1 recipient mice, equal numbers (1.5×10^5) of OT-1 *Ecsit*$^{fl/+}$ CD45.1.2 and *Ecsit*$^{fl/fl}$ *Rosa26*^{CreERT2} CD45.2 T_N cells were mixed and then i.v. transferred into CD45.1 recipient mice 1 d after implantation. The recipient mice were i.p. injected with tamoxifen from day 10 to day 15 to delete *Ecsit* in the *Ecsit*$^{fl/fl}$ *Rosa26*^{CreERT2} CD45.2 OT-1 T cells. To analyse OT-1 cells in TME, the recipient mice were killed for FACS analysis on day 20. For the in vivo DMF rescue experiments of memory T cell formation, the recipient mice (CD45.1) were treated with 10 mg kg^{-1} DMF every second day from day 11 to day 20. In some experiments, the mice were treated with 200 μg anti-PD-L1 on days 4 and 8 following tumour implantation and 10 mg kg^{-1} DMF daily.

Tcf7 overexpression in CD8$^+$ T cells

Plat-E cells were transfected with packaging plasmids (PGE) and *Tcf7*-MSCV-GFP plasmids (overexpression) using PolyJet reagent (SigmaGen) according to the manufacturer's instructions. The virus-containing supernatants were collected 48 h after transfection. Splenocytes from OT-1 mice were activated with OVA and IL-2 for 48 h in vitro and CD8$^+$ T cells were isolated by negative-selection magnetic beads. The CD8$^+$ T cells were mixed with the virus supernatant, centrifuged at a speed of 2,000*g* for 2 h at room temperature and then cultured in an incubator for another 4 h. The virus-containing supernatant was replaced with fresh RPMI 1640 medium supplemented with 10% heat-inactivated fetal calf serum, 2 mM L-glutamine, 1 mM sodium pyruvate, 10 mM HEPES, 5 mM β-mercaptoethanol and 1% penicillin and streptomycin. GFP-positive cells indicated TCF-1 OE.

Flow cytometry

Single-cell suspensions from the thymus, spleen and lymph nodes were generated after mashing tissue through a 70-μm cell strainer. Following treatment with red blood lysis buffer, the cell suspensions were surface stained using fluorescently labelled antibodies for FACS analysis. For the intracellular staining of IFN-γ and TNF-α, single tumour-cell suspensions were incubated in RPMI medium containing phorbol 12-myristate-13-acetate (1:2,000; MultiSciences, CS0001), ionomycin (1:1,000; MultiSciences, CS0002) and brefeldin A (1:1,000; eBioscience, 00-4506-51) for 4 h at 37 °C. After washing the samples with HBSS solution, surface proteins were stained, the cells were fixed and permeabilized using a Cytofix/Cytoperm kit (eBioscience, 88-8824-00) and finally intracellular IFN-γ and TNF-α were stained. For the transcription factor staining, the cells were fixed and permeabilized using a Foxp3/transcription factor staining buffer set (eBioscience, 00-5523-00), after which intranuclear transcription factors were stained.

For the tumour model, tumour tissues were weighed, cut into smaller pieces and suspended in 10 ml tumour digestion buffer (2% FBS, 0.5 mg ml^{-1} collagenase IV and 100 U ml^{-1} DNase I in RPMI medium). After digestion for 45 min at 37 °C with rotation (200 r.p.m.), the cell suspension was filtered through a 70-μm filter to obtain a single-cell suspension. Immune cells were isolated by density-gradient centrifugation using 40 and 80% Percoll (GE Healthcare). For the liver, liver tissues were cut into smaller pieces and suspended in 10 ml liver digestion buffer (2% FBS, 0.5 mg ml^{-1} collagenase IV, 0.5 mg ml^{-1} collagenase II and 100 U ml^{-1} DNase I in RPMI medium). Following digestion for 45 min at 37 °C with rotation (200 r.p.m.), the cell suspension was filtered through a 70-μm filter to obtain a single-cell suspension. Immune cells were isolated by density-gradient centrifugation using 40 and 70% Percoll. The immune cells were then stained using fluorescently labelled antibodies for FACS analysis. Intracellular staining of cytokines and transcription factors was performed as described earlier.

Antibodies and drugs

The following antibodies were used for FACS: anti-BCL-6–PerCP-eFluor 710 (BCL; eBioscience, 46-5453-82), anti-CD11b–FITC (M1/70; eBioscience, RM2801), anti-CD11c–PE (N418; eBioscience, 12-0114-82), anti-CD127–PE-Cyanine7 (A7R34; eBioscience, 25-1271-82), anti-CD25–PE (PC61.5; eBioscience, 12-0251-82), anti-CD44–AlexaFluor700 (IM7; eBioscience, 56-0441-82), anti-CD44–APC (IM7; eBioscience, 17044182), anti-CD44–FITC (IM7; eBioscience, 11-0441-82), anti-CD45.1–eFlour450 (A20; eBioscience, 48-0453-82), anti-CD45.2–PE-Cyanine7 (104; eBioscience, 25-0454-82), anti-CD45-AlexaFluor700 (30-F11; eBioscience, 56-0451-82), anti-CD4–PE-Cyanine7 (RM4-5; eBioscience, 25-2242-82), anti-CD62L–eFlour450 (MEL-14; eBioscience, 48062182), anti-CD8a–APC-Cyanine7 (53-6.7; BioLegend, 100714), anti-F4/80–APC (BM8; eBioscience, 17-4801-82), anti-Foxo-1–AlexaFluor488 (C29H4; Cell Signaling Technology, 58223S), anti-IFN-γ–PerCP-Cyanine5.5 (XMG1.2; eBioscience, 85-45-7311-82), anti-Ki67–APC (SolA15; eBioscience, 17-5698-82), anti-KLRG1–FITC (2F1; eBioscience, 11-5893-82), anti-Ly6C–PE-Cyanine7 (PK136; eBioscience, 25-5941-81), anti-Ly6G–eFlour450 (1A8; eBioscience, 48-9668-82), anti-NK1.1–PE-Cyanine7 (PK136; eBioscience, 25-5941-81), anti-PD-1–APC (J43; eBioscience, 17-9985-82), anti-SCA-1–APC (D7; eBioscience, 11-5981-82), anti-T-BET–BV421 (4B10; BioLegend, 644815), anti-TCF-1–APC (C63D9; Cell Signaling Technology, 37636S), anti-TIGIT–BV421 (1G9; BD, 565270), anti-TIM-3–PE-Cyanine7 (RMT3-23; eBioscience, 25-5870-80), anti-TNFα–APC (MP6-XT22; eBioscience, 17-7321-82), anti-CD16/CD32 (93; eBioscience, 14-0161-85), fixable viability dye–eFlour 506 (eBioscience, 65-0866-14), H-2K (b)/SIINFEKL Tetramer–PE (HELIXGEN) and mouse FITC–IgG isotype control (eBioscience, 31505), all of which were diluted 1:400 in staining buffer. The following antibodies were used for the western blots: anti-ECSIT (Novus, NBP1-91858; 1:2,000 dilution), anti-β-Actin (Sigma, A1978; 1:3,000 dilution), anti-TCF7 (Cell Signaling Technology, C46C7; 1:1,000 dilution), IRDye 800CW goat anti-rabbit IgG (LI-COR Biosciences, 926-32211; 1:3,000 dilution) and IRDye 680RD goat anti-rabbit IgG (LI-COR Biosciencese, 926-68070; 1:3,000 dilution). The following antibodies were used for ChIP–qPCR: anti-HA (BioLegend, 901514; 1:100 dilution) and anti-H3K4me3 (ABclonal, A2357; 1:100 dilution). The following drugs were used: anti-PD-L1 (BioXcell, BE0101) and DMF (MCE, HY-17363). The peptide fragment we used was $OVA_{257–264}$ peptide (GenScript, RP10611).

Immunoblot analysis

T cells were collected and lysed in NP-40 lysis buffer (50 mM Tris–HCl, pH 7.4, containing 150 mM NaCl, 1% (vol/vol) IGEPAL, 10% (wt/vol) glycerol, 50 mM NaF, 1 mM Na_3VO_4, 1 mM dithiothreitol and 1 mM phenylmethylsulphonyl fluoride) plus complete protease inhibitor 'cocktail' (Sigma-Aldrich) for 60 min at 4 °C. The lysates were centrifuged at 14,000*g* for 10 min. The supernatants were denatured with SDS buffer and boiled for 10 min. Proteins were separated by SDS–polyacrylamide gel electrophoresis and transferred onto nitrocellulose membranes. The membranes were immunoblotted with primary antibodies and proteins were detected with the appropriate secondary anti-rabbit conjugated to fluorophores. Immunoreactivity was visualized using the Odyssey imaging system (LI-COR Biosciences).

Extracellular flux analysis

A Seahorse XFe96 extracellular flux analyser (Agilent Technologies) was used according to the manufacturer's instructions to measure the OCR and ECAR rates. Briefly, splenocytes from *Ecsit*$^{fl/fl}$ and *Ecsit*$^{fl/fl}$ *dLck*-Cre OT-1 mice were activated with OVA and IL-2 in vitro for 48 h. CD8$^+$ T cells were isolated by negative-selection magnetic beads and cultured with IL-15 for 3 d to induce memory T cell differentiation. The OCR of memory CD8$^+$ T cells was analysed under basal conditions and after sequential injections of 1 mM oligomycin A, 1.5 mM carbonyl cyanide 4-(trifluoromethoxy) phenylhydrazone and 0.1 mM rotenone with 1 mM antimycin A. The ECAR was analysed under basal conditions and after sequential injections of 10 mM glucose, 1 mM oligomycin A and 50 mM 2-deoxyglucose.

RNA-seq and data analysis

Wild-type and iKO OT-1 cells were sorted for RNA-seq on day 35 after VSV-OVA infection or day 20 after B16F10-OVA tumour implantation. Total RNA was extracted using TRIzol (Life Technology, 15596018) according to the manufacturer's instructions. RNA isolation, library construction and sequencing were performed by LC-BIO TECHNOLOGIES. Clean reads were mapped to the mouse reference genome (mm10) using STAR (version 2.7.7a). The matched reads were calculated and then normalized to fragments per kilobase of transcript per million mapped reads for gene expression analysis. Fold changes were calculated for all possible comparisons and a 1.2-fold cutoff was used to select genes with expression changes. The GO and KEGG pathway enrichment analysis was performed by applying the online tool of DAVID Bioinformatics Resources 6.8 (http://david.ncifcrf.gov) using

significant DEGs (fold change > 1.2, $P < 0.05$) as target genes. The GSEA analysis was performed using the GSEA v4.1 software. Transcription factor enrichment analysis was performed using ChEA3 (https://maayanlab.cloud/chea3/) using significant DEGs (fold change > 1.2, $P < 0.05$) as target genes.

ATAC-seq and data analysis

Wild-type and iKO OT-1 cells were sorted on day 35 after VSV-OVA infection or day 20 after B16F10-OVA tumour implantation for ATAC-seq analysis. Ten thousand cells from each replicate were used to prepare ATAC-seq libraries using a TruePrep DNA library prep kit V2 for Illumina (Vazyme Biotech, TD502) according to the manufacturer's instructions and sequencing was performed by Novogene. The ATAC-seq reads were mapped to the mouse genome (mm10) using Bowtie 2 (version 2.2.9). To identify peaks with differential accessibility, we counted the duplicated reads overlapping with peaks. DESeq2 (version 1.16.0) was then used for statistical comparisons, using a similar procedure to that used for RNA-seq data analysis. Peaks with an adjusted $P < 0.05$ and fold change > 1.5 were considered to have differential accessibility. The online tool of DAVID Bioinformatics Resources 6.8 was used to perform GO and KEGG pathway enrichment analyses. The motif analysis was done using HOMER (version 4.9.1) and IGV (version 2.8.2) was used to visualize the data. The fold enrichment over 1.2 (the ratio of the percentage of target sequences with motif to the percentage of background sequences with motif) in WT or iKO cells with less than 1.2 in iKO or WTs were considered the special transcription factor.

Metabolite measurements and analysis

Mass spectrometry-based metabolomics were performed for OT-1 WT (*Ecsit*$^{fl/fl}$) and iKO (*Ecsit*$^{fl/fl}$ *Rosa26*^{CreERT2}) CD8$^+$ T cells from an in vitro culture system. The samples were analysed on an Ultimate 3000 (Dionex) ultra performance liquid chromatography system coupled to a Q Exactive HF (QE-HF) mass spectrometer (Thermo Fisher Scientific). Chromatographic separation was conducted using reversed-phase liquid chromatography separation with a Kinetex EVO C18 column (2.1 mm × 100 mm, 2.6 µm; Phenomenex) and hydrophilic-interaction liquid chromatography with an InfinityLab Poroshell 120 Hilic-Z column (2.1 mm × 100 mm, 2.7 µm; Agilent). Each sample was injected in a randomized fashion for analysis to avoid complications related to the injection order. For reversed-phase liquid chromatography analysis, the mobile phase consisted of phase A (0.1% formic acid in H_2O) and phase B (0.1% formic acid in acetonitrile) with a flow rate of 0.4 ml min^{-1}. The reversed-phase liquid chromatography elution conditions were as follows: 0 min, 10% phase B; 1 min, 30% phase B; 19 min, 95% phase B; 20 min, 95% phase B; 20.1 min, 10% phase B and 23 min, 10% phase B. For hydrophilic-interaction liquid chromatography analysis, mobile phase A was 25 mM CH_3COONH_4 and 25 mM NH_4OH in H_2O and mobile phase B was acetonitrile, which was run at a flow rate of 0.3 ml min^{-1}. The hydrophilic-interaction liquid chromatography elution conditions were as follows: 0 min, 85% phase B; 1 min, 85% phase B; 12 min, 65% phase B; 12.1 min, 40% phase B; 15 min, 40% phase; 15.1 min, 85% phase B and 20 min, 85% phase B. The temperature of the column chamber was set at 40 °C. The mass spectrometry was performed in a data-dependent acquisition mode ranging from m/z 70 to m/z 1,000 with a 60,000 resolution in both positive and negative modes simultaneously.

All of the MS raw data files were converted into mzML format using MSConvert (version 3.0). The MS-DIAL (version 4.36) software was used for deconvolution, peak picking, alignment and compound identification. The detailed parameter setting was as follows: MS1 tolerance, 0.01 Da; MS2 tolerance, 0.05 Da; minimum peak height, 10,000 amplitudes; mass slice width, 0.1 Da; smoothing method, linear weighted moving average; smoothing level, three scans; minimum peak width, five scans; sigma window value, 0.5; identification score cutoff, 70%; remove feature based on blank information; sample maximum / blank average, fivefold change. $[M + H]^+$, $[M + NH_4]^+$ and $[M + Na]^+$ were included in adduct ion setting for positive analysis, and $[M - H]^-$, $[M + FA\text{-}H]^-$, $[M + HAC\text{-}H]^-$ were included in the adduct ion setting for negative analysis (FA-H typically refers to the form of the target compound as the formate adduct ion (in negative ion mode); HAC-H typically represents the form of the target compound as the acetate adduct ion (in negative ion mode)). Missing data zero values were replaced with 1/10 of the minimum peak height over all samples. Values were normalized to the cell number (total ion current). A Student's t-test was used to compare continuous variables between two groups. The SIMCA software (version 14.1; Umetrics) was employed for PCA analysis. The variable importance in $P < 0.05$ of each metabolite was used as the combined cutoff of the statistical significance. Visualization of metabolomics was conducted using the R package and GraphPad Prism (version 8.0.2).

Confocal microscopy assay

OT-1 *Ecsit*$^{fl/fl}$ (WT) and *Ecsit*$^{fl/fl}$ *dLck*-Cre memory CD8$^+$ T cells from an in vitro culture system were collected and then stained with MitoTracker Red for 30 min in culture medium. The cells were washed twice with PBS and stained with Hoechst solution (1:10,000 dilution) for 10 min. Next, the cells were centrifuged at 1,500 r.p.m. for 10 min, the supernatant was discarded and the cells were resuspended in PBS. The cells were placed on a glass slide and covered with a coverslip. Confocal fluorescence images were acquired with a Zeiss LSM 800 confocal microscope, and images were processed and analysed using the ZEN 2012 software.

Transmission electron microscopy

OT-1 *Ecsit*$^{fl/fl}$ (WT) and *Ecsit*$^{fl/fl}$ *dLck*-Cre memory CD8$^+$ T cells from an in vitro culture system were collected and fixed with 2.5% glutaraldehyde for 48 h, rinsed with phosphate buffer and postfixed with 1% osmium tetroxide. Next, the samples were rinsed and dehydrated in ethanol and acetone. The samples were then embedded in Spurr resin. Ultrathin sections were then stained with 2% uranyl acetate and lead citrate, and visualized using an FEI Tecnai G2 Spirit Bio TWIN electron microscope.

ChIP assays

For ChIP–seq, the DNA was end polished and dA tailed by adding End-repair and A-tailing reaction mix (Vazyme, N103-01 and N101-01) directly to the PCR tube and incubating the sample at 28 °C for 15 min and 68 °C for 15 min. Adaptors (0.6 µM; TransNGS Adapter for Illumina, KI241) containing barcodes were ligated to the DNA fragments. The DNA libraries were amplified using the following PCR programme: 98 °C for 3 min; 14–15 cycles of 98 °C for 30 s, 60 °C for 30 s and 72 °C for 30 s; and 72 °C for 3 min, followed by a hold at 10 °C. The library was purified and selected with DNA Clean beads (Vazyme, N411-01). The quality of the amplified libraries for sequencing was verified using a PerkinElmer LabChip GX Touch and StepOnePlus Real-Time PCR system. Sequencing was then performed on an Illumina Novaseq 6000 platform in PE150 mode.

Raw ChIP–seq reads were first subjected to adaptor trimming and low-quality read filtering using flexbar (version 2.5) with the following parameters: -u 5 -m 26 -ae RIGHT -at 2 -ao 1. The trimmed reads were mapped to the mouse reference genome (mm10) using Bowtie 2 (version 2.2.9) with default parameters. Reads that mapped to mitochondrial DNA or that had low mapping quality (<30) were excluded from the downstream analysis. Duplicate reads due to PCR amplification of single DNA fragments during library preparation were identified using Picard (version 2.17.3; available at http://broadinstitute.github.io/picard) and thus removed from the downstream analysis. Peak calling was performed using MACS2 (version 2.2.7.1) in narrow-peak mode with the parameters -p 0.01–bdg–SPMR. To compare data between different conditions, the de-duplicated H3K4me3 reads overlapping with peaks

were counted and then normalized using library scale factors estimated using the deepTools suite (version 3.5.0). DESeq2 (version 1.30.0) was then used for statistical comparisons, using a procedure similar to that used for the RNA-seq data. The gene rank analysis was based on the Z-statistic of differential H3K4me3 levels ($P < 0.05$).

ChIP–qPCR assays

The assay was performed following the standard protocol. Briefly, WT (*Ecsit*$^{fl/fl}$ OT-1) and iKO (*Ecsit*$^{fl/fl}$ *Rosa26*^{CreERT2} OT-1) memory or exhausted CD8$^+$ T cells from an in vitro culture system treated with or without DMF were crosslinked in 1% formaldehyde for 10 min at 25 °C, quenched with 0.125 M glycine for 5 min at 25 °C and lysed in 0.2% SDS with a protease inhibitor tablet for 10 min on ice. The genomic DNA was then fragmented by sonication to shear the chromatin to 200–500 bp. The sheared crosslinked chromatin was incubated overnight with primary or IgG antibodies, followed by an incubation with Protein A/G beads. DNA purification was performed using a ChIP DNA clean concentrator (Beyotime, D0033) according to the manufacturer's instructions. The precipitated DNA was amplified using primers and quantified an a StepOnePlus real-time PCR machine using Hieff qPCR SYBR Green master mix (Yeasen) according to the manufacturer's instructions. The *Tcf7* qPCR primer sequences were: F, 5′-AGACCTAATCTTTTCCGTT-3′ and R, 5′-CTGATTCACGTTGCTGAC-3′. The *Tcf7* qPCR primers were purchased from Sangon Biotech.

Kdm5 activity assay

Cells (2×10^6) were resuspended in 400 µl cell lysis buffer (10 mM HEPES pH 7.5, 10 mM KCl, 0.1 mM EDTA, 1 mM dithiothreitol, 0.5% Nonidet-40 and 0.5 mM phenylmethylsulfonyl fluoride along with a protease inhibitor cocktail) and allowed to swell on ice for 20 min with intermittent mixing. The tubes were vortexed and then centrifuged at 12,000*g* and 4 °C for 10 min. The pelleted nuclei were washed twice with the cell lysis buffer, resuspended in 25 ml ice-cold nuclear extraction buffer (20 mM HEPES, 400 mM NaCl, 1 mM EDTA, 1 mM dithiothreitol and 1 mM phenylmethylsulfonyl fluoride with protease inhibitor cocktail) and incubated in ice for 30 min with intermittent sonication. The nuclear extracts were collected by centrifugation at 12,000*g* and 4 °C for 15 min. The supernatant was used immediately in a colorimetric KDM5/JARID activity quantification assay kit (Abnova) according to the manufacturer's instructions.

Analysis of data from public database

To explore the role of ECSIT in immune cells, we analysed the expression of *Ecsit* in immune cells from publicly available gene and protein databases such as ImmGen (https://www.immgen.org/) and BioGPS (http://biogps.org/). To explore the role of ECSIT in CD8$^+$ T cells in acute or chronic stimulation, we analysed the public data from GEO accession numbers GSE157072 (ref. 51), GSE84105 (ref. 52), GSE123235 (ref. 53), GSE120575 (ref. 54) and GSE166181 (ref. 55). We investigated the correlation of gene expression profiles between *ECSIT* and immune checkpoints through the TISIDB web portal (http://cis.hku.hk/TISIDB/index.php). To explore the peak of TCF-1 target genes in CUT&RUN data of CD8$^+$ T cells in acute or chronic stimulation, we analysed the public data from GSE177064 (ref. 56) and GSE139056 (ref. 57). To investigate the characteristics of CD8$^+$ T cells as indicated by RNA-seq data during acute or chronic stimulation, we analysed the public data from GSE23321 (ref. 31), GSE164978 (ref. 58), GSE122969 (ref. 59) and GSE9650 (ref. 60). To explore the relationship between the survival rate of patients and *ECSIT*, we used the Gene Expression Profiling Interactive Analysis 2 (GEPIA2) platform (http://gepia2.cancer-pku.cn/). A log-rank test was used for statistical analysis.

Statistics and reproducibility

Information about the statistical details and methods used is provided in the figure legends. Statistical analysis was performed using GraphPad Prism 8.0 or 9.0. A two-way analysis of variance test was used for tumour growth. A log-rank test was used for the mice survival curves. Other statistical analyses were performed using a two-tailed unpaired Student's *t*-test, unless stated otherwise. Data normality was not assumed. All statistical tests were two-sided, unless specified otherwise. Sample sizes were not pre-determined using statistical methods but followed those reported previously[33] and no data were excluded from the analyses. Biological samples were excluded from the study only in cases where the sample preparation or data acquisition was unsuccessful. The experiments were not randomized, and data collection and analysis were not performed blind to the conditions of the experiments, except for tumour size and mice survival analysis.

Reporting summary

Further information on research design is available in the Nature Portfolio Reporting Summary linked to this article.

Data availability

RNA-seq, ATAC-seq and ChIP–seq data that support the findings of this study have been deposited in the NCBI Sequence Read Archive database under the NCBI Bioproject accession codes PRJNA905206, PRJNA902096, PRJNA905582, PRJNA904827 and PRJNA1016360. Source data are provided with this paper.

References

51. Milner, J. J. et al. Delineation of a molecularly distinct terminally differentiated memory CD8 T cell population. *Proc. Natl Acad. Sci. USA* **117**, 25667–25678 (2020).
52. Im, S. J. et al. Defining CD8$^+$ T cells that provide the proliferative burst after PD-1 therapy. *Nature* **537**, 417–421 (2016).
53. Miller, B. C. et al. Subsets of exhausted CD8$^+$ T cells differentially mediate tumor control and respond to checkpoint blockade. *Nat. Immunol.* **20**, 326–336 (2019).
54. Sade-Feldman, M. et al. Defining T cell states associated with response to checkpoint immunotherapy in melanoma. *Cell* **175**, 998–1013 (2018).
55. De Biasi, S. et al. Circulating mucosal-associated invariant T cells identify patients responding to anti-PD-1 therapy. *Nat. Commun.* **12**, 1669 (2021).
56. Shan, Q. et al. Tcf1 preprograms the mobilization of glycolysis in central memory CD8$^+$ T cells during recall responses. *Nat. Immunol.* **23**, 386–398 (2022).
57. Shan, Q. et al. Ectopic Tcf1 expression instills a stem-like program in exhausted CD8$^+$ T cells to enhance viral and tumor immunity. *Cell. Mol. Immunol.* **18**, 1262–1277 (2021).
58. Pritykin, Y. et al. A unified atlas of CD8 T cell dysfunctional states in cancer and infection. *Mol. Cell* **81**, 2477–2493 (2021).
59. Kurtulus, S. et al. Checkpoint blockade immunotherapy induces dynamic changes in PD-1$^-$ CD8$^+$ tumor-infiltrating T cells. *Immunity* **50**, 181–194 (2019).
60. Wherry, E. J. et al. Molecular signature of CD8$^+$ T cell exhaustion during chronic viral infection. *Immunity* **27**, 670–684 (2007).
61. Jolma, A. et al. Multiplexed massively parallel SELEX for characterization of human transcription factor binding specificities. *Genome Res.* **20**, 861–873 (2010).

Acknowledgements

We thank L. Lu (Zhejiang University, Hangzhou, China), X. Zhang (Huazhong University of Science and Technology, Wuhan, China), H. Wang (ShanghaiTech University, Shanghai, China), X. Wang (Nanjing Medical University, Nanjing, China) and Y. Xiao (Shanghai Institute of Nutrition and Health, Chinese Academy of Sciences) for providing *dLck*-Cre, *Rosa26*^{CreERT2}, OT-1, CD45.1 and *Rag1*$^{-/-}$ mice respectively. We thank C. Xu (Institute of Biochemistry and Cell Biology, Chinese Academy of Sciences) for providing B16F10 and

B16F10-OVA cells. We also thank C. Y. Yang (Sun Yat-sen University, Zhongshan School of Medicine, Guangzhou, China) for providing VSV-OVA and LM-OVA. This work was supported by the National Key Research and Development Program of China (grant number 2022YFA1303900 to S.Y.), National Natural Science Foundation of China (grant numbers 32270921 and 82070567 to S.Y., 32170742 to X.W. and 82204354 to Y.H.), the Start Fund for Specially Appointed Professor of Jiangsu Province (S.Y. and X.W.), the Open Project of State Key Laboratory of Reproductive Medicine of Nanjing Medical University (grant number SKLRM-2021B3 to S.Y.), the talent cultivation project of 'Organized scientific research' of Nanjing Medical University (grant number NJMURC20220014 to S.Y.), the Start Fund for High-level Talents of Nanjing Medical University (grant number NMUR2020009 to X.W.), the Open Project of Chinese Materia Medica First-Class Discipline of Nanjing University of Chinese Medicine (grant number 2020YLXK017 to B.W.), the Priority Academic Program Development of Jiangsu Higher Education Institutions (to B.W.), the Natural Science Foundation of Jiangsu Province (grant number BK20221352 to B.W.), the Jiangsu Provincial Outstanding Postdoctoral Program (grant number 2022ZB419 to Y.H.) and the Postdoctoral Research Funding Project of Gusu School (grant number GSBSHKY202104 to Y.H.). F.H. is supported by a Charles Hood Child Health Grant.

Author contributions

Y.Y., Y.W., Z.W., H.Y., Y.G., Y.H., Y.J., S.W. and F.X. designed and performed the experiments, analysed the data and prepared the figures. F.H., Y.C. and X.W. provided the key technique mentoring, data analysis and research resources. B.W. and F.H. contributed to the experimental design and edited the manuscript. S.Y. supervised the project. Y.Y., Y.W. and S.Y. wrote the manuscript.

Competing interests

The authors declare no competing interests.

Additional information

Extended data is available for this paper at https://doi.org/10.1038/s41556-024-01351-9.

Supplementary information The online version contains supplementary material available at https://doi.org/10.1038/s41556-024-01351-9.

Correspondence and requests for materials should be addressed to Fiachra Humphries, Yun Chen, Xi Wang or Shuo Yang.

Peer review information *Nature Cell Biology* thanks Ping-Chih Ho, Laura Mackay and the other, anonymous, reviewer(s) for their contribution to the peer review of this work. Peer reviewer reports are available.

https://doi.org/10.1038/s41556-024-01351-9

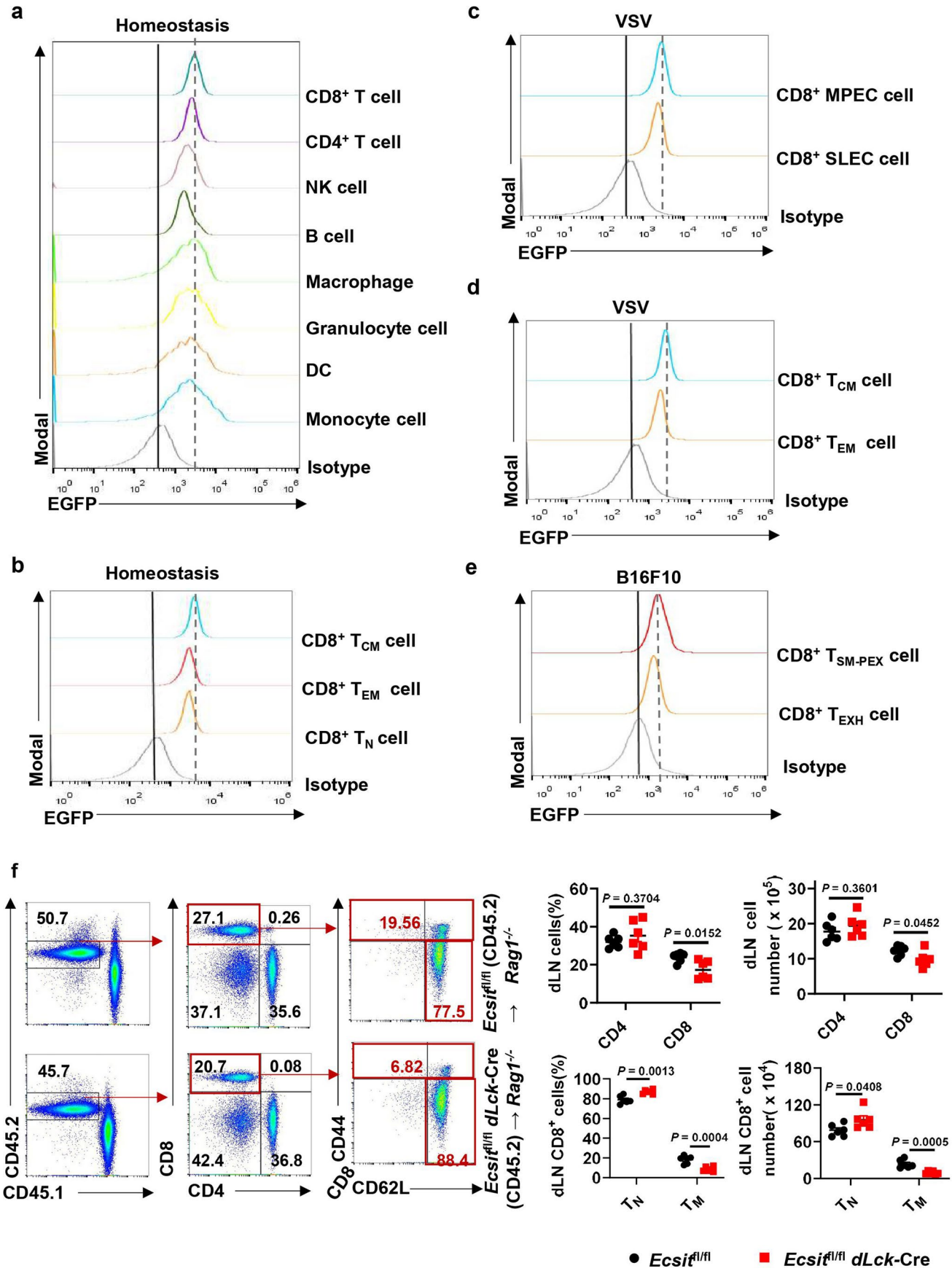

Extended Data Fig. 1 | See next page for caption.

https://doi.org/10.1038/s41556-024-01351-9

Extended Data Fig. 1 | ECSIT is upregulated in memory CD8$^+$ T cells, and promotes memory CD8$^+$ T cells generation in a cell-intrinsic manner under the homeostasis. (a) Representative flow cytometry plots of *Ecsit*−EGFP expression in immune cells in Fig. 1d. **(b)** Representative flow cytometry plots of *Ecsit*−EGFP expression in T_N, $T_{CM,}$ and T_{EM} of CD8$^+$ T cells in Fig. 1e. **(c)** Representative flow cytometry plots of *Ecsit*−EGFP expression in MPEC and SLEC of CD8$^+$ T cells in Fig. 1f. **(d)** Representative flow cytometry plots of *Ecsit*−EGFP expression in T_{EM} and T_{CM} of CD8$^+$ T cells in Fig. 1g. **(e)** Representative flow cytometry plots of *Ecsit*−EGFP expression in T_{SCMP} and T_{EXH} of CD8$^+$ T cells in Fig. 1h. **(f)** CD45.1 mice bone marrows were mixed equally with *Ecsit*$^{fl/fl}$ or *Ecsit*$^{fl/fl}$ *dLck*-Cre (CD45.2) mice bone marrows then injected intravenously into irradiated *Rag1*$^{-/-}$ mice. 8 weeks later, draining lymph nodes were collected and analysed by flow cytometry for CD4$^+$ T cells, CD8$^+$ T cells, and CD8$^+$ T_N, T_M cells. Data are pooled from three independent experiments and n = 6 for (f). Error bars show mean ± sem. Two-tailed unpaired student's *t*-test for (f).

https://doi.org/10.1038/s41556-024-01351-9

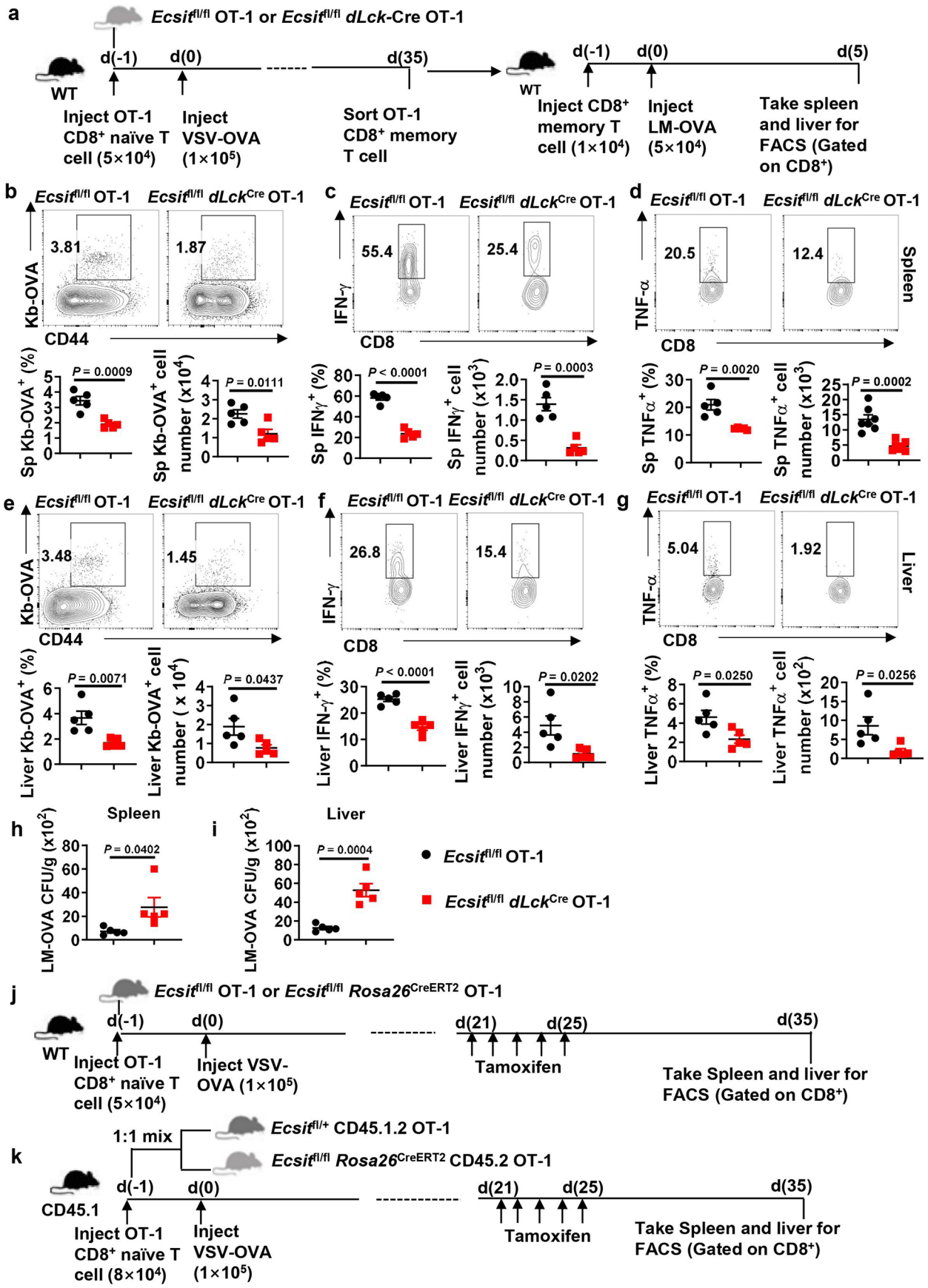

Extended Data Fig. 2 | See next page for caption.

https://doi.org/10.1038/s41556-024-01351-9

Extended Data Fig. 2 | ECSIT promotes the recall response of memory CD8$^+$ T cells. (a) Schematic of memory CD8$^+$ T cells recall response. Naive CD8$^+$ T cells obtained from *Ecsit*$^{fl/fl}$ OT-1 or *Ecsit*$^{fl/fl}$ *dLck*-Cre OT-1 mice were transferred into WT recipient mice. Subsequently, the recipient mice were infected with VSV-OVA 1 day later. After 35 days, memory OT-1 T cells were sorted and transferred into naive WT recipient mice, followed by LM-OVA challenge. Spleen and liver were collected for analyses 5 days later. **(b, e)** Representative flow cytometry plots (top) and the analysis of percentage and number (bottom) of Kb-OVA$^+$ CD44$^+$ CD8$^+$ cells in the spleen **(b)** and liver **(e)**. **(c, d, f, g)** Representative flow cytometry plots (top) and the analysis of percentage and number (bottom) of IFN-γ$^+$ **(c)** and TNF-α$^+$ **(d)** T cells gated on Kb-OVA$^+$ CD44$^+$ CD8$^+$ cells in the spleen, and IFN-γ$^+$ **(f)** and TNF-α$^+$ **(g)** T cells gated on Kb-OVA$^+$ CD44$^+$ CD8$^+$ cells in the liver. **(h, i)** Bacterial load of LM-OVA in the spleen **(h)** and liver **(i)**. **(j)** Schematic of memory T cells formation in acute infection. Naive CD8$^+$ T cells from *Ecsit*$^{fl/fl}$ OT-1 or *Ecsit*$^{fl/fl}$ *Rosa26*^{CreERT2} OT-1 mice were transferred into WT recipient mice, followed by VSV-OVA infection 1 day later. Tamoxifen was intraperitoneally injected from day21 to day25. OT-1 memory cells were analysed on day35. **(k)** Schematic of memory T cells formation in acute infection with adaptive co-transplantation model. Naive CD8$^+$ T cells from *Ecsit*$^{fl/+}$ CD45.1.2 OT-1 and *Ecsit*$^{fl/fl}$ *Rosa26*^{CreERT2} CD45.2 OT-1 mice were mixed equally and transferred into CD45.1 recipient mice, and then the recipient mice were infected with VSV-OVA 1 day later. Tamoxifen was intraperitoneally injected from day21 to day25. OT-1 memory cells were analysed on day35. Data are pooled from three independent experiments and n = 5 for (b-i). Error bars show mean ± sem. Two-tailed unpaired student's *t*-test for (b-i).

https://doi.org/10.1038/s41556-024-01351-9

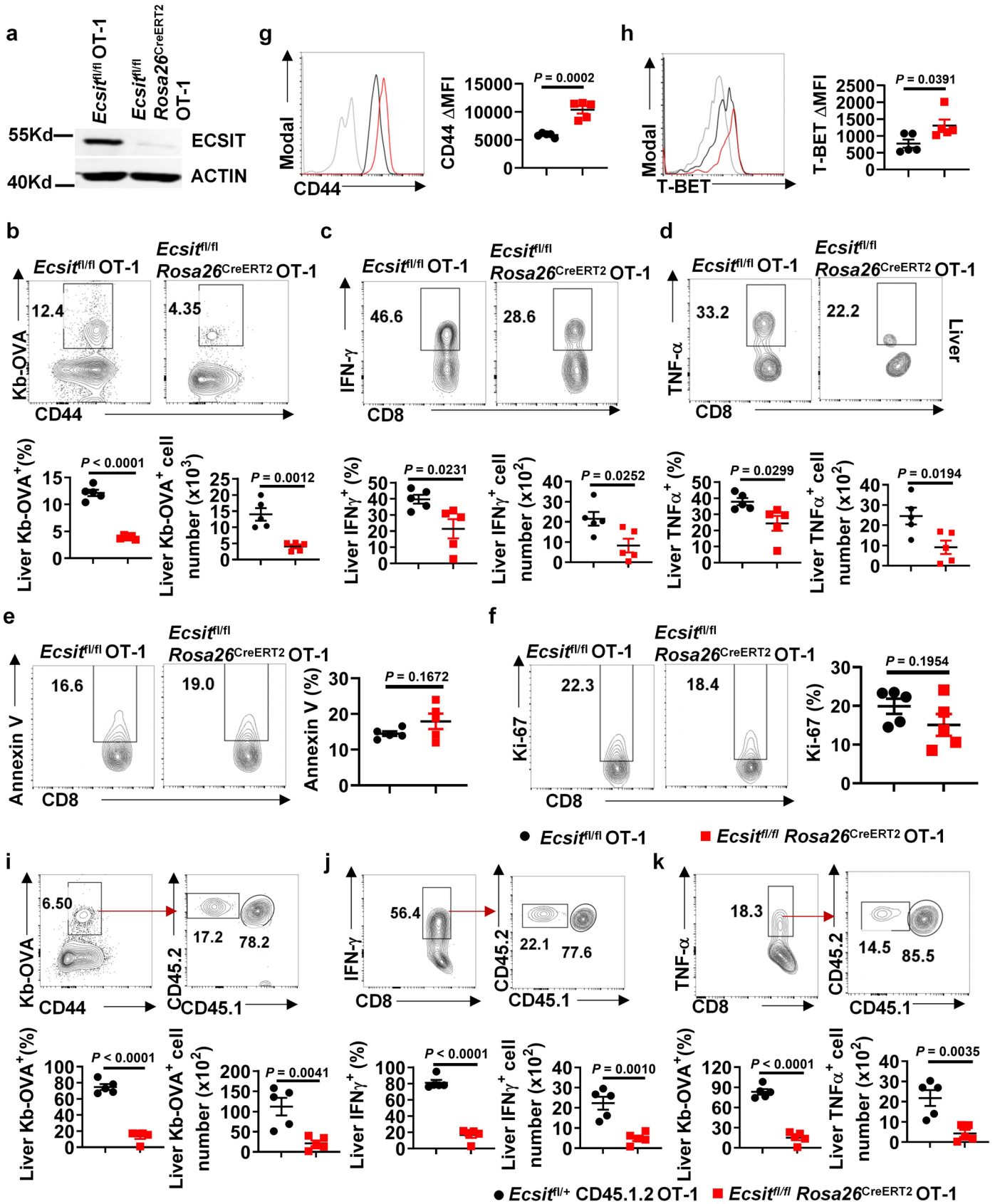

Extended Data Fig. 3 | See next page for caption.

https://doi.org/10.1038/s41556-024-01351-9

Extended Data Fig. 3 | ECSIT deficiency impairs memory CD8$^+$ T cells formation and function without affecting proliferation and apoptosis during acute viral infection. **(a)** Immunoblot analysis of ECSIT expression in *Ecsit*$^{fl/fl}$ OT-1 and *Ecsit*$^{fl/fl}$ *Rosa26*^{CreERT2} OT-1 cells 35 days after VSV-OVA infection. **(b)** Representative flow cytometry plots (top) and the analysis of percentage and number (bottom) of Kb-OVA$^+$ CD44$^+$ CD8$^+$ cells in the liver. **(c, d)** Representative flow cytometry plots and the analysis of percentage and number of IFN-γ$^+$ **(c)** and TNF-α$^+$ **(d)** T cells gated on Kb-OVA$^+$ CD44$^+$ CD8$^+$ cells in the liver. **(e, f)** Representative flow cytometry plots (left) and the analysis of percentage and number (right) of Annexin V$^+$ **(e)** and Ki-67$^+$ **(f)** in Kb-OVA$^+$ CD44$^+$ CD8$^+$ cells in the spleen. **(g, h)** Flow cytometry analysis of CD44 **(g)** and T-BET **(h)** expression in Kb-OVA$^+$ CD44$^+$ CD8$^+$ cells in the liver. **(i)** Representative flow cytometry plots (top) and the analysis of percentage and number (bottom) of *Ecsit*$^{fl/+}$ CD45.1.2 OT-1 and *Ecsit*$^{fl/fl}$ *Rosa26*^{CreERT2} CD45.2 OT-1 cells gated on Kb-OVA$^+$ CD44$^+$ CD8$^+$ cells in the spleen. **(j, k)** Representative flow cytometry plots (top) and the analysis of percentage and number (bottom) of *Ecsit*$^{fl/+}$ CD45.1.2 OT-1 and *Ecsit*$^{fl/fl}$ *Rosa26*^{CreERT2} CD45.2 OT-1 cells gated on Kb-OVA$^+$ CD44$^+$ CD8$^+$ IFN-γ$^+$ **(j)** and TNF-α$^+$ **(k)** T cells in the liver. Data are pooled from three independent experiments for (a-k), and n = 5 for (b-k). Error bars show mean ± sem. Two-tailed unpaired student's *t*-test for (b-k).

https://doi.org/10.1038/s41556-024-01351-9

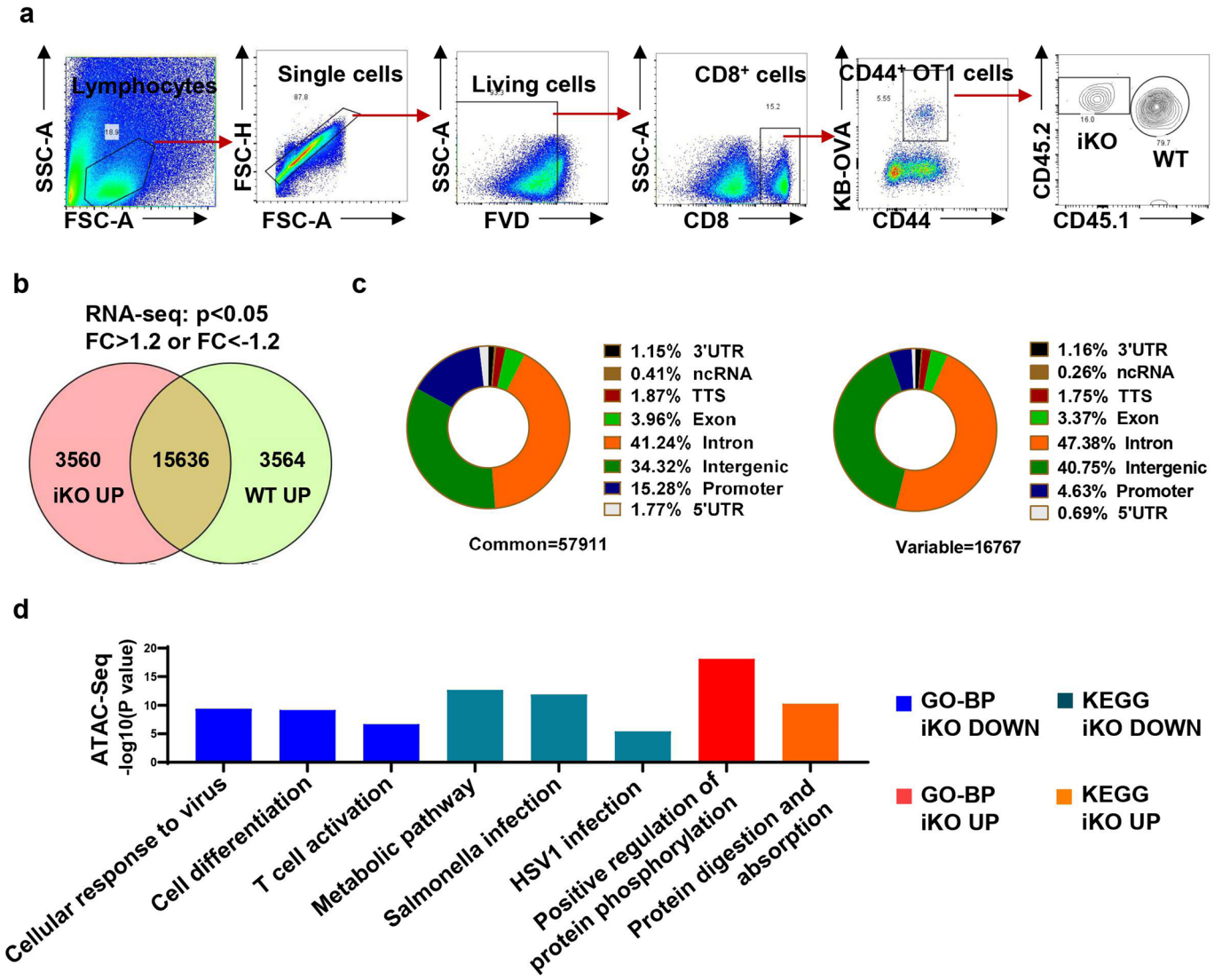

Extended Data Fig. 4 | ECSIT affects chromatin accessibility of memory CD8⁺ T cells and promotes transcription regulation of *Tcf7* during acute viral infection. **(a)** Flow cytometry gating strategy of sorting *Ecsit*$^{fl/+}$ CD45.1.2 OT-1 and *Ecsit*$^{fl/fl}$ *Rosa26*^{CreERT2} CD45.2 OT-1 cells (memory) from CD45.1 recipient mice 35 days after VSV-OVA infection for RNA-seq and ATAC-seq. **(b)** Venn diagrams of differentially and commonly expressed genes between *Ecsit*$^{fl/+}$ CD45.1.2 OT-1 and *Ecsit*$^{fl/fl}$ *Rosa26*^{CreERT2} CD45.2 OT-1 cells. **(c)** Pie charts of the genomic distribution of differentially and commonly accessible chromatin regions between *Ecsit*$^{fl/+}$ CD45.1.2 OT-1 and *Ecsit*$^{fl/fl}$ *Rosa26*^{CreERT2} CD45.2 OT-1 cells. **(d)** GO and KEGG analysis of differentially accessible chromatin region genes. **(e)** Genome track view of the *Ccr7* and *Slamf6* locus showing ATAC-seq and *Tcf7* ChIP–seq peaks (GSE177064). *Tcf7* predictive binding sites (red shadows) are listed. One-side Fisher's Exact test for (b, d).

https://doi.org/10.1038/s41556-024-01351-9

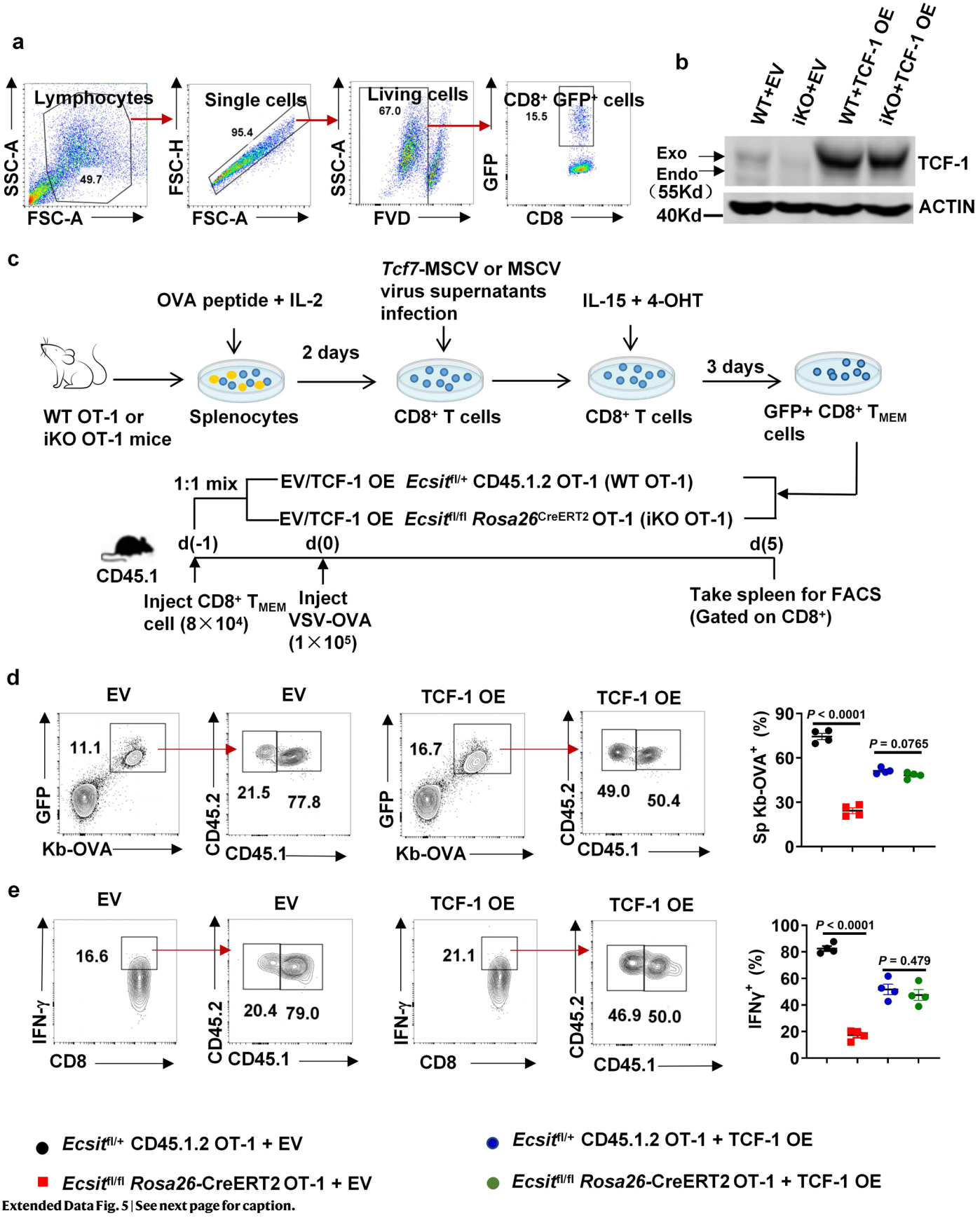

Extended Data Fig. 5 | See next page for caption.

https://doi.org/10.1038/s41556-024-01351-9

Extended Data Fig. 5 | TCF-1 overexpression promotes memory T cells formation in ECSIT deficiency CD8$^+$ T cells in vitro. (a, b) *Ecsit*$^{fl/fl}$ OT-1 (WT) and *Ecsit*$^{fl/fl}$ *Rosa26*^{CreERT2} OT-1 (iKO) splenocytes were activated with OVA and IL-2 for 2 days, followed by sorting of CD8$^+$ T cells, then CD8$^+$ T cells were transduced with vector (EV) or TCF-1 (TCF-1 OE) by the retroviral system and cultured in IL-15 for 3 days to induce IL-15-mediated differentiation of memory T cells in the presence of 4$^-$OHT. **(a)** Flow cytometry gating strategy of TCF-1 overexpression CD8$^+$ T cells. **(b)** Immunoblot analysis of ECSIT expression in WT + EV, WT + TCF-1 OE, iKO+EV and iKO+TCF-1 OE cells. **(c)** Schematic of the experiments. *Ecsit*$^{fl/+}$ CD45.1.2 OT-1(WT) and *Ecsit*$^{fl/fl}$ *Rosa26*^{CreERT2} CD45.2 OT-1(iKO) mice splenocytes were activated with OVA and IL-2 for 2 days, followed by sorting of CD8$^+$T cells, then CD8$^+$T cells were transduced with vector (EV) or TCF-1 (TCF-1 OE) by the retroviral system and cultured in IL-15 for 3 days to induce IL-15-mediated differentiation of memory T cells in the presence of 4-OHT. WT and iKO memory CD8$^+$T (GFP$^+$) were mixed at a 1:1 ratio and transferred into CD45.1 recipient mice, and then the recipient mice were infected with VSV-OVA 1 day later. OT-1 cells were analysed on day 5 after infection in the spleen. **(d, e)** Representative flow cytometry plots (left) and the analysis of percentage (right) of OT-1 cells (GFP$^+$ Kb-OVA$^+$ CD44$^+$ CD8$^+$ T) **(d)** and IFN-γ$^+$ cells **(e)** gated on GFP$^+$ Kb-OVA$^+$ CD44$^+$ CD8$^+$ T cells in the spleen. Data are pooled from two independent experiments and n = 4 for (d-e). Error bars show mean ± sem. ***P ≤ 0.001, ns, not significant. Two-tailed unpaired student's t-test for (d-e).

https://doi.org/10.1038/s41556-024-01351-9

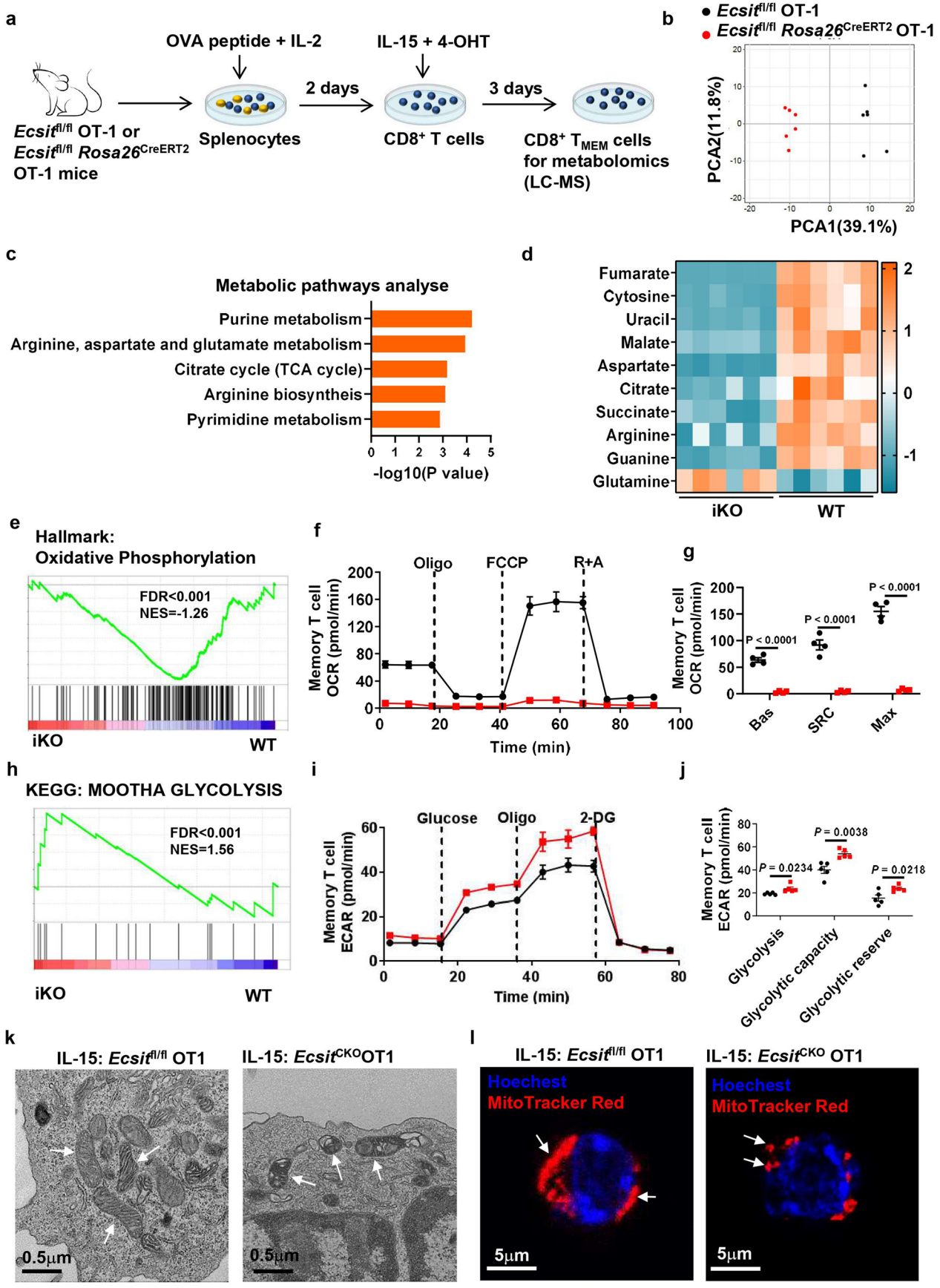

Extended Data Fig. 6 | See next page for caption.

https://doi.org/10.1038/s41556-024-01351-9

Extended Data Fig. 6 | ECSIT deficiency dysregulates mitochondrial metabolism and inhibits fumarate production. (a-d) *Ecsit*$^{fl/fl}$ OT-1 (WT) and *Ecsit*$^{fl/fl}$ *Rosa26*^{CreERT2} OT-1 (iKO) splenocytes were activated with OVA and IL-2 for 2 days, followed by sorting of CD8$^+$ T cells, then cultured in IL-15 for 3 days to induce IL-15-mediated differentiation of memory T cells in the presence of 4-OHT. Memory T cells were collected for metabolite detection. **(a)** Schematic of memory CD8$^+$ T cells induced in vitro. **(b)** PCA analysis of metabolomics data. **(c)** Pathway enrichment analysis of changed metabolites. **(d)** Heat map of relative abundance of significantly changed metabolites. **(e)** GSEA analysis of oxidative Phosphorylation genes (Hallmark) with RNA-seq data. **(f,g,k,l)** *Ecsit*$^{fl/fl}$ OT-1 and *Ecsit*$^{fl/fl}$ *dLck*-Cre OT-1 (CKO) splenocytes were activated with OVA and IL-2 for 2 days, followed by sorting of CD8$^+$ T cells, then CD8$^+$ T cells were cultured in IL-15 for 3 days to induce IL-15-mediated differentiation of memory T cells. **(f, g)** Seahorse extracellular flux analysis of OCR; n = 4 biological replicates per group. **(k)** Transmission electron microscope images of mitochondria. **(l)** Confocal microscopy images of mitochondria. Mitochondria are red (MitoTracker Red) and nuclei are blue (Hoechst). **(h)** GSEA analysis of MOOTHA GLYCOLYSIS Pathway (KEGG) with RNA-seq data. **(i-j)** *Ecsit*$^{fl/fl}$ OT-1 and *Ecsit*$^{fl/fl}$ *dLck*-Cre OT-1 (CKO) splenocytes were activated with OVA and IL-2 for 2 days, followed by sorting of CD8$^+$ T cells, then CD8$^+$ T cells were cultured in IL-15 for 3 days to induce IL-15-mediated differentiation of memory T cells. Memory T cells were collected for Seahorse extracellular flux analysis of ECAR. Data are pooled from three independent experiments for (f, g, i-l), and n = 4 for (f, g) or 5 for (I, j) Error bars show mean ± sem. One-side Fisher's Exact test for (c). Two-tailed unpaired student's *t*-test for (g, j).

https://doi.org/10.1038/s41556-024-01351-9

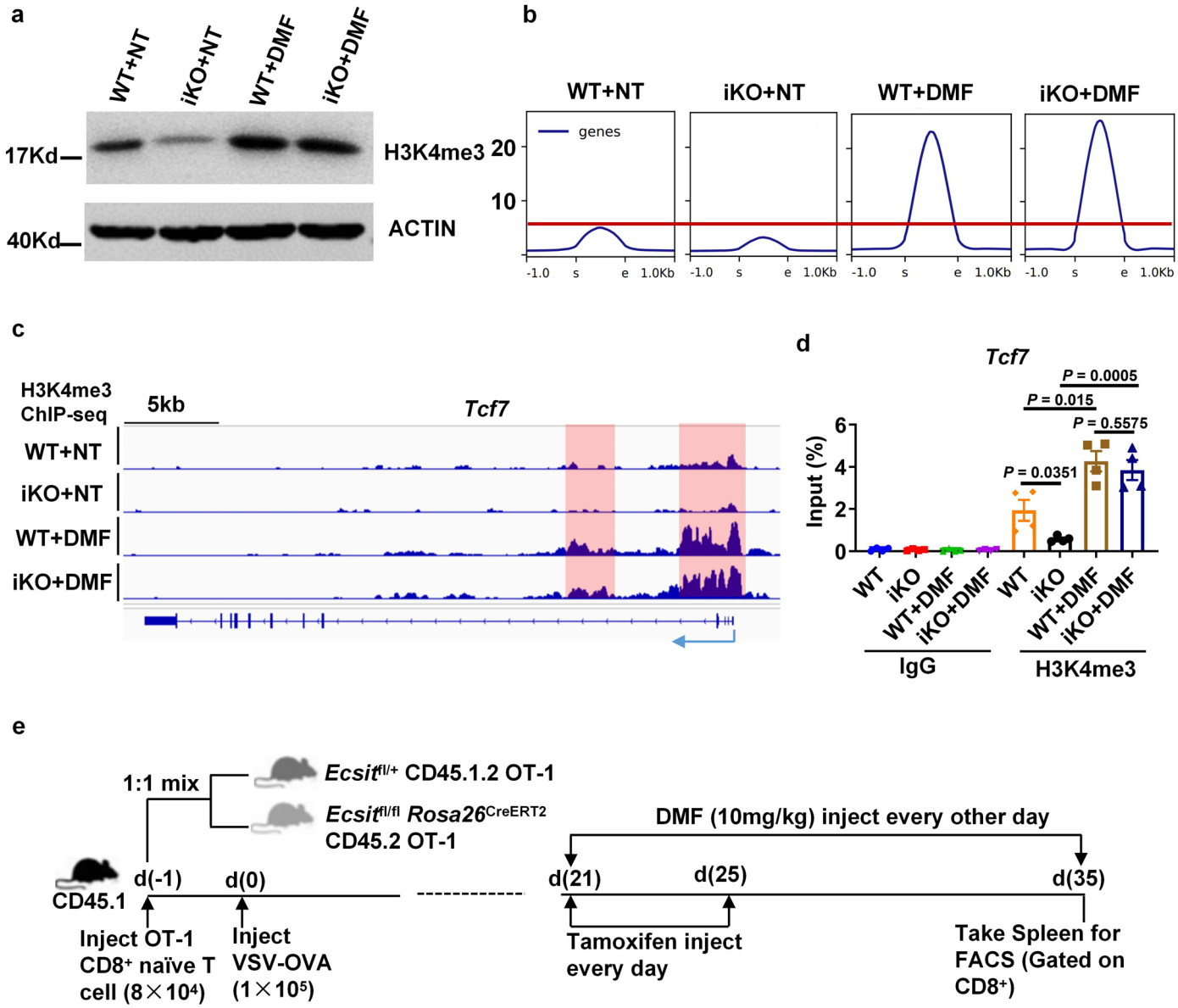

Extended Data Fig. 7 | DMF supplement significantly rescue H3K4me3 modification and H3K4me3 level at the *Tcf7* promoters of ECSIT-deficient memory CD8⁺ T cells. (a) Immunoblot analysis of H3K4me3 expression in WT + NT, WT + DMF, iKO+NT and iKO + DMF memory T cells induced in vitro. **(b)** Comparison of entire H3K4me3 ChIP–seq peaks in WT + NT, WT + DMF, iKO + NT and iKO + DMF memory T cells induced in vitro. **(c)** Genome track view of the *Tcf7* locus showing H3K4me3 ChIP–seq peaks in WT + NT, WT + DMF, iKO + NT and iKO + DMF memory T cells induced in vitro. H3K4me3 predictive binding sites (red shadows) are listed. **(d)** ChIP–qPCR analysis of H3K4me3 levels at the promoters of *Tcf7* in WT + NT, WT + DMF, iKO + NT and iKO + DMF memory T cells induced in vitro; n = 4 biological replicates per group. **(e)** Schematic of memory T cells formation with DMF supplement in acute infection. The equal number of OT-1 naive CD8⁺ T cells from *Ecsit*$^{fl/+}$ CD45.1.2 OT-1 and *Ecsit*$^{fl/fl}$ *Rosa26*^{CreERT2} CD45.2 OT-1 mice were mixed and transferred into CD45.1 recipient mice, and then the recipient mice were infected with VSV-OVA 1 day later. Tamoxifen was administered every day for five treatments starting at day 21 to day 25, and DMF was also injected every other day from day 21 to day 35. OT-1 memory cells from the spleen were analysed on day 35. Data are pooled from three independent experiments for (a, d), and n = 4 for (d). Error bars show mean ± sem. Two-tailed unpaired student's *t*-test for (d).

https://doi.org/10.1038/s41556-024-01351-9

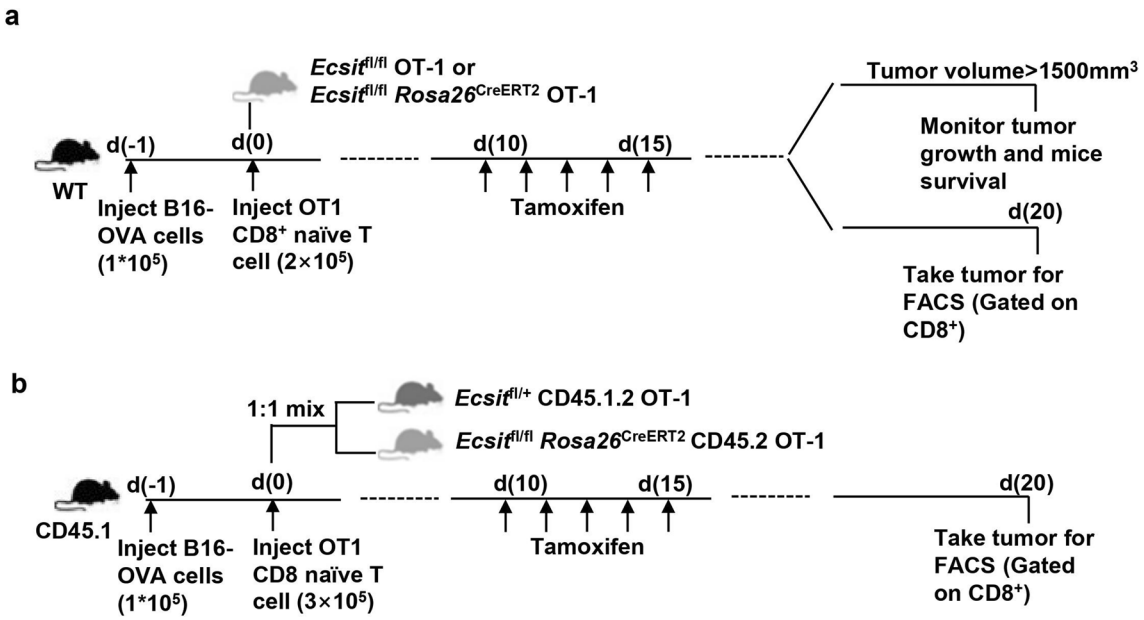

Extended Data Fig. 8 | ECSIT deficiency impairs CD8⁺ T cells antitumour function through cell-intrinsic mechanisms. (a) Schematic of tumour model. WT recipient mice were implanted subcutaneously with B16F10-OVA cells, and then *Ecsit*$^{fl/fl}$ OT-1 or *Ecsit*$^{fl/fl}$ *Rosa26*^{CreERT2} OT-1 naive CD8⁺ T cells were transferred into recipient mice 1 day later. Tamoxifen was injected intraperitoneally 5 times from day10 to day15. The growth of B16F10-OVA melanomas and the survival of mice were assessed. And transferred OT-1 cells were analysed on day 20. **(b)** Schematic of tumour model with adaptive co-transplantation. CD45.1 recipient mice were implanted subcutaneously with B16F10-OVA cells, and then *Ecsit*$^{fl/+}$ CD45.1.2 OT-1 and *Ecsit*$^{fl/fl}$ *Rosa26*^{CreERT2} CD45.2 OT-1 naive CD8⁺ T cells were mixed and transferred into recipient mice 1 day later. Tamoxifen was injected intraperitoneally 5 times from day10 to day15. Transferred OT-1 cells were analysed on day 20.

https://doi.org/10.1038/s41556-024-01351-9

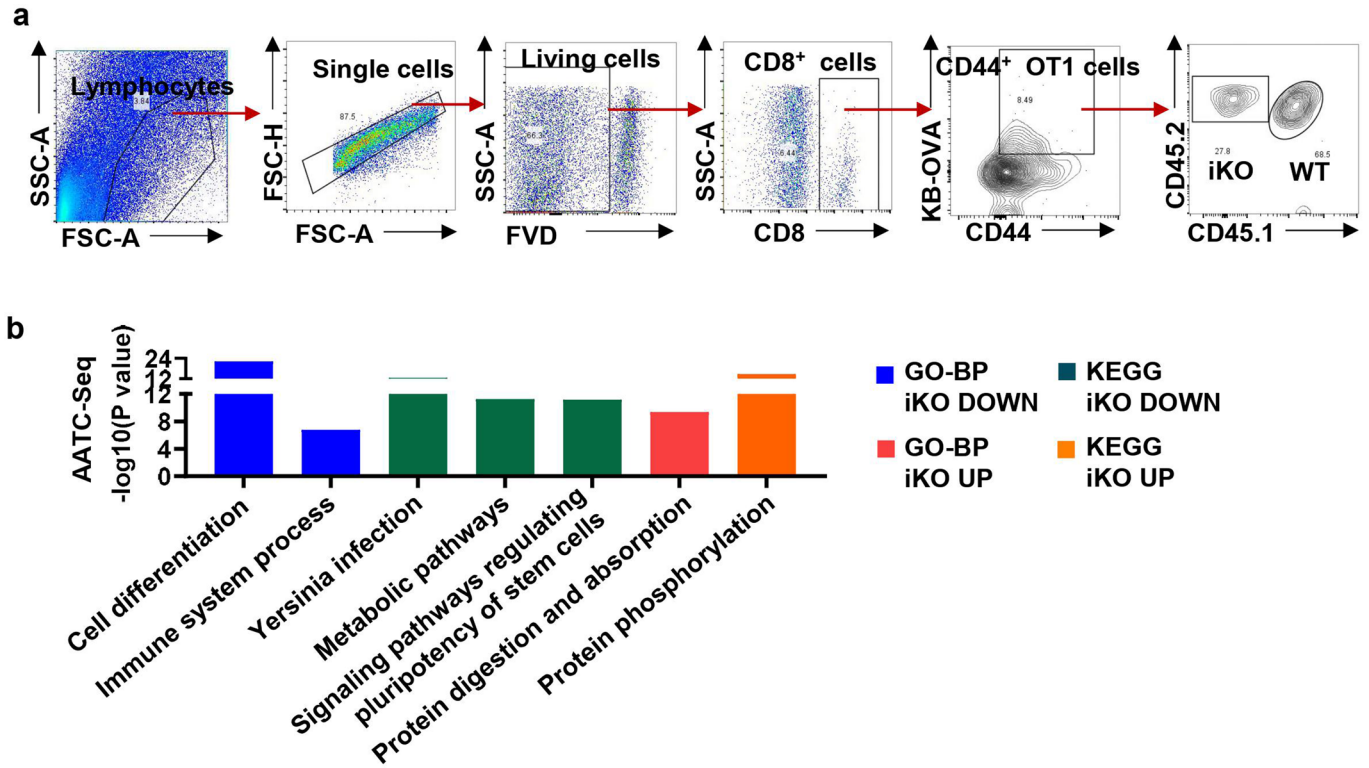

Extended Data Fig. 9 | ECSIT affects chromatin accessibility of TME CD8⁺ T cells and promotes transcription regulation of *Tcf7* in chronic tumour stimulation. (a) Flow cytometry gating strategy of sorting *Ecsit*$^{fl/+}$ CD45.1.2 OT-1 and *Ecsit*$^{fl/fl}$ *Rosa26*^{CreERT2} CD45.2 OT-1 cells (memory) from B16F10-OVA tumour-bearing CD45.1 recipient mice for RNA-seq and ATAC-seq. **(b)** GO and KEGG analysis of differentially accessible chromatin region genes. **(c)** Genome track view of the *Ccr7* and *Slamf6* locus showing ATAC-seq and *Tcf7* CUT&RUN peaks (GSE139056). *Tcf7* predictive binding sites (red shadows) are listed. One-side Fisher's exact test for (b).

https://doi.org/10.1038/s41556-024-01351-9

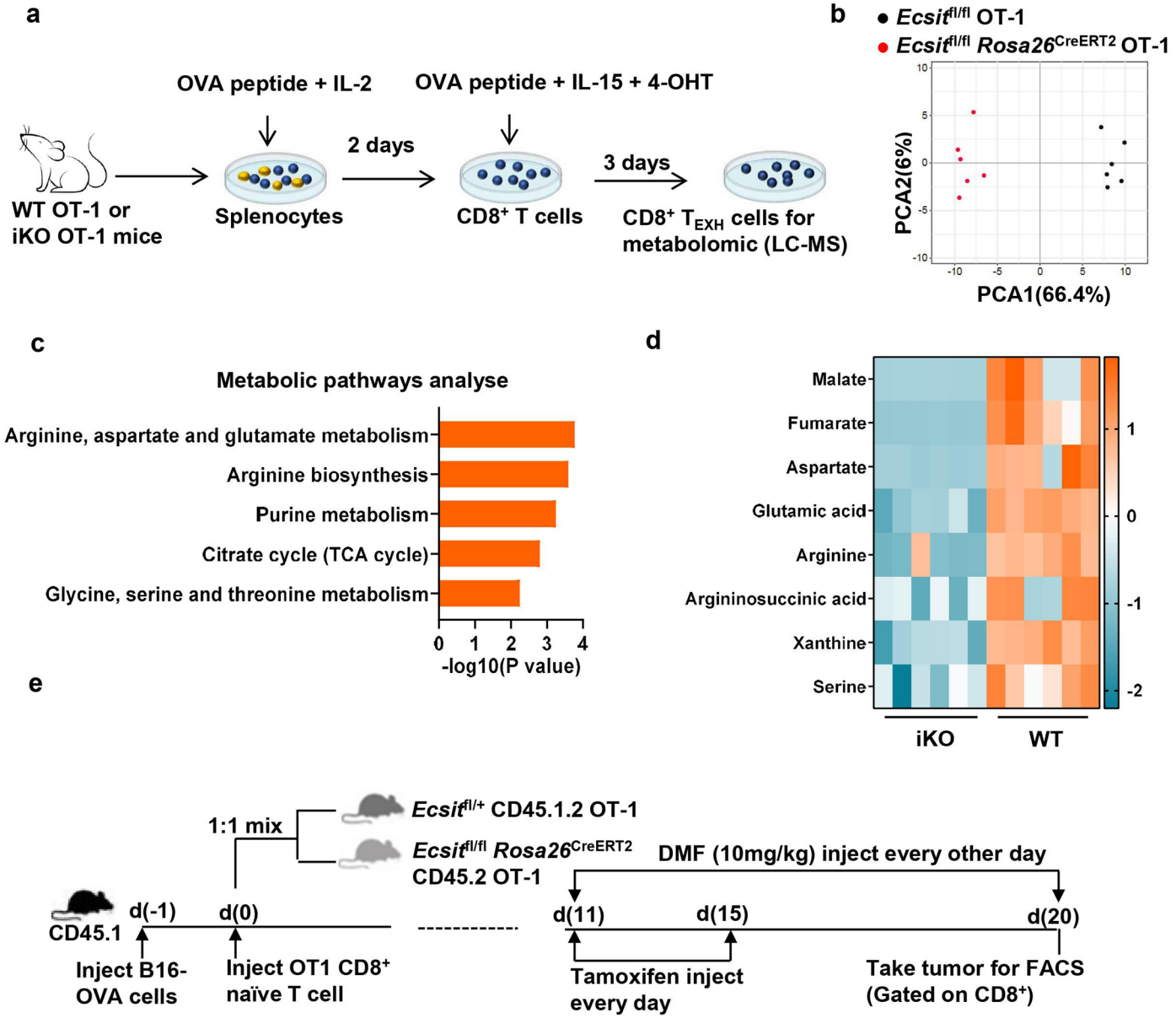

Extended Data Fig. 10 | ECSIT deficiency inhibits fumarate production of CD8⁺ memory T cells in chronic stimulation, and DMF supplementation improves the antitumour function of ECSIT-deficient memory CD8⁺ T cells in vivo. (a-d) *Ecsit*$^{fl/fl}$ OT-1 (WT) and *Ecsit*$^{fl/fl}$ *Rosa26*^{CreERT2} OT-1 (iKO) splenocytes were activated with OVA and IL-2 for 2 days, followed by sorting of CD8⁺ T cells, and then sorted CD8⁺ T cells were cultured in IL-15 and OVA for 3 days to mimic tumour antigen chronic stimulation in the presence of 4-OHT. CD8⁺ T cells were collected for metabolite detection. **(a)** Schematic of CD8⁺ T cells stimulated chronically in vitro. **(b)** PCA analysis of metabolomics data. **(c)** Pathway enrichment analysis of changed metabolites. **(d)** Heat map of relative abundance of significantly changed metabolites. **(e)** Schematic of tumour model with DMF supplement. An equal number of OT-1 naive CD8⁺ T cells from *Ecsit*$^{fl/+}$ CD45.1.2 OT-1 and *Ecsit*$^{fl/fl}$ *Rosa26*^{CreERT2} CD45.2 OT-1 mice were mixed and transferred into CD45.1 recipient mice that had been engrafted with B16F10-OVA melanoma cells. Tamoxifen was administered every day for five treatments starting at day 11 to day 15 and DMF was also injected every other day from day 11 to day 20. OT-1 cells from the tumour were analysed on day 20. One-side Fisher's exact test for (c).

nature portfolio

Corresponding author(s): Shuo Yang

Last updated by author(s): Dec 1, 2023

Reporting Summary

Nature Portfolio wishes to improve the reproducibility of the work that we publish. This form provides structure for consistency and transparency in reporting. For further information on Nature Portfolio policies, see our Editorial Policies and the Editorial Policy Checklist.

Statistics

For all statistical analyses, confirm that the following items are present in the figure legend, table legend, main text, or Methods section.

n/a	Confirmed
☐	☒ The exact sample size (*n*) for each experimental group/condition, given as a discrete number and unit of measurement
☐	☒ A statement on whether measurements were taken from distinct samples or whether the same sample was measured repeatedly
☐	☒ The statistical test(s) used AND whether they are one- or two-sided *Only common tests should be described solely by name; describe more complex techniques in the Methods section.*
☐	☒ A description of all covariates tested
☐	☒ A description of any assumptions or corrections, such as tests of normality and adjustment for multiple comparisons
☐	☒ A full description of the statistical parameters including central tendency (e.g. means) or other basic estimates (e.g. regression coefficient) AND variation (e.g. standard deviation) or associated estimates of uncertainty (e.g. confidence intervals)
☐	☒ For null hypothesis testing, the test statistic (e.g. *F*, *t*, *r*) with confidence intervals, effect sizes, degrees of freedom and *P* value noted *Give P values as exact values whenever suitable.*
☒	☐ For Bayesian analysis, information on the choice of priors and Markov chain Monte Carlo settings
☒	☐ For hierarchical and complex designs, identification of the appropriate level for tests and full reporting of outcomes
☒	☐ Estimates of effect sizes (e.g. Cohen's *d*, Pearson's *r*), indicating how they were calculated

Our web collection on statistics for biologists contains articles on many of the points above.

Software and code

Policy information about availability of computer code

Data collection	Images for Immunofluorescence were acquired on Zeiss LSM 800 confocal microscope with ZEN 2012 software and were exported as the .tif files. Flow cytometry data were acquired with Attune NxT flow cytometer with Acoustic Focusing Cytometer software (Thermo fisher), and were exported as the .fcs files. Western Blot data was obtained using LI-COR oddysey. OCR and ECAR data was measured using a Seahorse XFe96 extracellular flux analyzer (Agilent Technologies). Bulk RNA-seq data was obtained using LC-BIO TECHNOLOGIES. OMNI ATAC-seq data was obtained using TruePrep DNA Library Prep Kit V2 (Vazyme Biotech Co.,Ltd, TD502) and Novogene for Illumina Metabolism data was measured using analyzed on an Ultra Performance Liquid Chromatography (UPLC) Ultimate 3000 system (Dionex, Germering, Germany) coupled to a Q Exactive HF (QE-HF) mass spectrometry (Thermo Fisher Scientific, Bremen, Germany). ChIP-seq data was obtained using ChIP Assay Kit (beyotime, P2078) and Illumina Novaseq 6000. Transmission electron microscope images were obtained using FEI Tecnai G2 Spirit Bio TWIN electron microscope.
Data analysis	Statistical tests were performed using Graph Pad Prism 9.0 software and are presented as the means ± SEM. To analyze imaging data, Fiji (version 1.0) was used. Flow cytometry analysis was performed using Flow Jo 10.0.7 software. Software used to analyze the bulk RNA-Seq, OMNI ATAC-seq, ChIP-seq and metabolism data include R statistical environment (v4.0.3) and Cellranger (v3.1.0), R packages: Seurat (version 3.1.4); GSEA (version 4.1); DESeq2 (version 1.16.0); HOMER (version 4.9.1); IGV (version 2.8.2); MSConvert (version 3.0); MS-DIAL (version 4.36); SIMCA software (version 14.1); Flexbar (version 2.5); DESeq2 (version 1.30.0); Bowtie 2 (version 2.2.9); Picard (version 2.17.3); MACS2 (version 2.2.7.1).

For manuscripts utilizing custom algorithms or software that are central to the research but not yet described in published literature, software must be made available to editors and reviewers. We strongly encourage code deposition in a community repository (e.g. GitHub). See the Nature Portfolio guidelines for submitting code & software for further information.

Data

Policy information about availability of data

All manuscripts must include a data availability statement. This statement should provide the following information, where applicable:

- Accession codes, unique identifiers, or web links for publicly available datasets
- A description of any restrictions on data availability
- For clinical datasets or third party data, please ensure that the statement adheres to our policy

The RNA-seq, ATAC-seq and ChIP-seq data generated in this study have been deposited in the NCBI Sequence Read Archive (SRA) database under the NCBI Bioproject PRJNA905206, PRJNA902096, PRJNA905582, PRJNA904827 and PRJNA1016360.
For Metabolomics data, metabolite abundance between samples can be found in Supplementary Table.

Field-specific reporting

Please select the one below that is the best fit for your research. If you are not sure, read the appropriate sections before making your selection.

☒ Life sciences ☐ Behavioural & social sciences ☐ Ecological, evolutionary & environmental sciences

For a reference copy of the document with all sections, see nature.com/documents/nr-reporting-summary-flat.pdf

Life sciences study design

All studies must disclose on these points even when the disclosure is negative.

Sample size	No statistics were used to pre-determine sample size, and at least two independent experiments were conducted to ensure adequate reproducibility of results. For infection experiments, we routinely used 4 mice per genotype and condition at least, which allow for statistically valid comparisons based on perious publication (PMID: 32989328). For in vitro experiments, we used 4 biological replicates as in perious publication (PMID: 31871320). For ATAC-seq, bulk RNA-seq, ChIP-seq and LC-MS, minimum 3 biological replicates were used based on perious publications (PMID: 33574619, PMID: 34860557).
Data exclusions	No data were excluded.
Replication	All experiments were reliably reproduced. All reported data were from at least two independent experiments (each specified in figure legends) with exactly the same conditions established from pilot experiments.
Randomization	For in vivo experiments, sex and age-matched mice were distributed randomly for each experiment according to their genotypes. For in vitro experiments, samples and cells were grouped according to genotype or treatment.
Blinding	For the tumor size and mice survival analysis, the assessment were conducted in a blinded fashion. For FACS, qPCR analysis, samples were collected and performed by automated methods.

Reporting for specific materials, systems and methods

We require information from authors about some types of materials, experimental systems and methods used in many studies. Here, indicate whether each material, system or method listed is relevant to your study. If you are not sure if a list item applies to your research, read the appropriate section before selecting a response.

Materials & experimental systems

n/a	Involved in the study
☐	☒ Antibodies
☐	☒ Eukaryotic cell lines
☒	☐ Palaeontology and archaeology
☐	☒ Animals and other organisms
☒	☐ Human research participants
☒	☐ Clinical data
☒	☐ Dual use research of concern

Methods

n/a	Involved in the study
☐	☒ ChIP-seq
☐	☒ Flow cytometry
☒	☐ MRI-based neuroimaging

Antibodies

Antibodies used	The following antibodies were used for flow cytometry: Anti-BCL6-PerCP-eFluor 710 (BCL, eBioscience, 46-5453-82), anti-CD11b-FITC (M1/70, eBioscience, RM2801), anti-CD11c-PE (N418, eBioscience, 12-0114-82), anti-CD127-PE-CY7 (A7R34, eBioscience, 25-1271-82), anti-CD25-PE (PC61.5, eBioscience, 12-0251-82), anti-CD44-AlexaFluor700 (IM7, eBioscience,56-0441-82), anti-CD44-APC (IM7, eBioscience, 17044182), anti-CD44-FITC (IM7,

eBioscience, 11-0441-82), anti-CD45.1-eFlour450 (A20, eBioscience, 48-0453-82), anti-CD45.2-PE-CY7 (104, eBioscience, 25-0454-82), anti-CD45-AF700 (30-F11, eBioscience, 56-0451-82), anti-CD4-PE-CY7 (RM4-5, eBioscience, 25-2242-82), anti-CD62L-eFlour450 (MEL-14, eBioscience, 48062182), anti-CD8a-APC-CY7 (53-6.7, Biolegend, 100714), anti-F4/80-APC (BM8, eBioscience, 17-4801-82), anti-Foxo-1-AlexaFluro488 (C29H4, CST, 58223S), anti-IFNg-PerCP-Cyanine5.5 (XMG1.2, eBioscience, 85-45-7311-82), anti-Ki67-APC (SolA15, eBioscience, 17-5698-82), anti-KLRG1-FITC (2F1, eBioscience, 11-5893-82), anti-Ly6C-PE-CY7 (PK136, eBioscience, 25-5941-81), anti-Ly6G-eFlour450 (1A8, eBioscience, 48-9668-82), anti-NK1.1-PE-CY7 (PK136, eBioscience, 25-5941-81), anti-PD1-APC (J43, eBioscience, 17-9985-82), anti-SCA1-APC (D7, eBioscience, 11-5981-82), anti-T-BET-BV421 (4B10, Biolegend, 644815), anti-TCF1-APC (C63D9, CST, 37636S), anti-TIGIT-BV421 (1G9, BD, 565270), anti-TIM3-PECY7 (RMT3-23, eBioscience, 25-5870-80), anti-TNFa-APC (MP6-XT22, eBioscience, 17-7321-82), anti-CD16/CD32 (93, eBioscience, 14-0161-85), Fixable Viability Dye-eFlour 506 (eBioscience, 65-0866-14), H-2K (b)/SIINFEKL Tetramer-PE (HELIXGEN), Mouse FITC-IgG Isotype Control (eBioscience, 31505) all diluted in staining buffer (1:400).
The following antibodies were used for Immunoblotting:
Anti-ECSIT (Novus, NBP1-91858; 1:2000 dilution), anti-b-Actin (Sigma, A1978; 1:3000 dilution), anti-TCF7(CST, C46C7; 1:1000 dilution) , IRDye 800CW Goat anti-Rabbit IgG (LI-COR Biosciencese, 926-32211; 1:3000 dilution), IRDye 680RD Goat anti-Rabbit IgG (LI-COR Biosciencese, 926-68070; 1:3000 dilution).
The following antibodies were used for ChIP-qPCR:
Anti-HA (Biolegend, 901514; 1:100 dilution), anti-H3K4me3 (ABclonal, A2357;1:100 dilution).

Validation

All antibodies used were commercially available and have been validated by vendors as indicated on their webside. FC block was added to all FACS stainings to reduce non-specific staining. Antibodies for WB were validated by molecular weights of their target proteins.

Eukaryotic cell lines

Policy information about cell lines

Cell line source(s)

The C57BL/6-derived melanoma B16F10 and B16F10-OVA cells (originally obtained from the American Type Culture Collection) were provided by Dr. Chenqi Xu (Institute of Biochemistry and Cell Biology, Chinese Academy of Sciences), Plat-E cells were provided by Dr. Xiaoming Wang (Nanjing Medical University, China)

Authentication

None of the cell lines have been authenticated

Mycoplasma contamination

All cell lines were tested negative for mycoplasma contamination.

Commonly misidentified lines
(See ICLAC register)

No commonly misidentified cell lines were used.

Animals and other organisms

Policy information about studies involving animals; ARRIVE guidelines recommended for reporting animal research

Laboratory animals

All mice were on the C57BL/6 genetic background except for CD45.1, which is B6.SJL background. Ecsit fl/fl mice were generated by CRISPR/Cas9-mediated genome engineering by Biocytogen (Beijing, China), respectively. Two sgRNAs were designed by the CRISPR design tool (http://crispr.mit.edu) to target either a region upstream or downstream of the exon 4 and then were screened for on-target activity using a Universal CRISPR Activity Assay. Ecsit-EGFP was generated by CRISPR/Cas9-mediated genome engineering by Cyagen Biosciences (Guangzhou, China). The gRNA to mouse Ecsit gene, the donor vector containing the "3×Flag-2A-EGFP" cassette, and Cas9 mRNA were co-injected into fertilized mouse eggs to generate targeted conditional knockin offspring. F0 founder animals were identified by PCR followed by sequence analysis, bred to wild -type mice to test germline transmission and F1 animal generation.
To obtain mature T cell-conditional Ecsit knockout mice, Ecsit fl/fl mice were crossed with dLck-Cre mice (kindly gifted by Dr. Linrong Lu, Zhejiang University, China). Ecsit floxed mice were also crossed with Rosa26 CreERT2 mice (kindly gifted by Dr. Xinjun Zhang, Huazhong University of Science and Technology, China), to generate tamoxifen-induced Ecsit knockout mice (Ecsit fl/fl Rosa26CreERT2). Ecsit fl/fl, Ecsit fl/fl dLck-Cre, and Ecsit fl/fl Rosa26 CreERT2 mice were crossed with OT-1 mice (kindly gifted by Dr. Haopeng Wang, ShanghaiTech University, China) to generate Ecsit fl/fl, Ecsit fl/fl dLck-Cre and Ecsit fl/fl Rosa26 CreERT2mice especially responded to OVA257-264 (Ecsit fl/fl OT-1, Ecsit fl/fl dLck-Cre OT-1 and Ecsit fl/fl Rosa26 CreERT2 OT-1). Ecsit fl/fl OT-1 mice were crossed with CD45.1mice (kindly gifted by Dr. Xiaoming Wang, Nanjing Medical University, China), to obtain Ecsit fl/+ CD45.1.2 OT-1 mice. Rag1-/- (kindly gifted by Dr. Yichuan Xiao, Shanghai Institute of Nutrition and Health, University of Chinese Academy of Sciences, China).
All experiments were performed with adult male mice (8-12 weeks old). All mice were kept in a barrier facility with 12h dark/12h light cycles. at 19–23 °C and 45-65% humidity with water and food provided. All animal experiments were conducted in accordance with the procedure approved by the Ethical Review Committee for Laboratory Animal Welfare of Nanjing Medical University and the Nanjing University of Chinese Medicine.

Wild animals

This study did not involve the use of wild animals.

Field-collected samples

This study did not involve the use of field-collected samples.

Ethics oversight

All animal experiments were conducted in accordance with local guidelines and approved by the Ethical Review Committee for Laboratory Animal Welfare of the Nanjing Medical University and Nanjing University of Chinese Medicine.

Note that full information on the approval of the study protocol must also be provided in the manuscript.

ChIP-seq

Data deposition

☒ Confirm that both raw and final processed data have been deposited in a public database such as GEO.

☒ Confirm that you have deposited or provided access to graph files (e.g. BED files) for the called peaks.

Data access links *May remain private before publication.*	The ChIP-seq data generated in this paper have been deposited in the NCBI Sequence Read Archive (SRA) database under the NCBI Bioproject PRJNA1016360 that is publicly accessible at https://dataview.ncbi.nlm.nih.gov/object/PRJNA1016360?reviewer=r34sn0uqo30lj4usqdc5d303jl. The processed data is publicly accessible at 10.6084/m9.figshare.24143634
Files in database submission	WT_wDMF_2_R1.fastq.gz, WT_wDMF_2_R2.fastq.gz, WT_woDMF_IgG_2_R1.fastq.gz, WT_woDMF_IgG_2_R2.fastq.gz, WT_wDMF_1_R1.fastq.gz, WT_wDMF_1_R2.fastq.gz, KO wDMF_IgG_1_R1.fastq.gz, KO_wDMF_IgG_1_R2.fastq.gz, KO_wDMF_IgG_2_R1.fastq.gz, KO_wDMF_IgG_2_R2.fastq.gz, KO_woDMF_IgG_2_R1.fastq.gz, KO_woDMF_IgG_2_R2.fastq.gz, KO woDMF_2_R1.fastq.gz, KO_woDMF_2_R2.fastq.gz, KO_woDMF_IgG_1_R1.fastq.gz, KO_woDMF_IgG_1_R2.fastq.gz, KO woDMF_1_R1.fastq.gz, KO_woDMF_1_R2.fastq.gz, KO wDMF_1_R1.fastq.gz, KO_wDMF_1_R2.fastq.gz, WT woDMF 2 R1.fastq.gz, WT woDMF_2_R2.fastq.gz, KO wDMF_2_R1.fastq.gz, KO_wDMF_2_R2.fastq.gz, WT_woDMF_1_R1.fastq.gz, WT_woDMF_1_R2.fastq.gz, WT_wDMF_IgG 1_R1.fastq.gz, WT_wDMF_IgG_1_R2.fastq.gz, WT_wDMF_IgG_2_R1.fastq.gz, WT_wDMF_IgG_2_R2.fastq.gz
Genome browser session (e.g. UCSC)	10.6084/m9.figshare.24143634

Methodology

Replicates	2 replicates for each ChIP-seq sample
Sequencing depth	On average, ~100 million reads for the ChIP libraries, ~50 million reads for the IgG control libraries. Reads were 150 * 2 paired-ended.
Antibodies	Anti-HA (Biolegend, 901514), anti-H3K4me3 (ABclonal, A2357).
Peak calling parameters	bowtie2 -p 8 -X 2000 --mm -x mm10.bt2_index -1 ${ID}.1.fastq.gz -2 ${ID}.2.fastq.gz 2>$ID.bowtie2.log | samtools view -h -uS - | samtools sort -@ 2 -m 2G - -o $ID.bam samtools view -h -F 12 $ID.bam | grep -v 'chrM' | samtools view -Sb - > $ID.fltM.bam java -jar $Picard MarkDuplicates I=$ID.fltM.bam O=$ID.dedup.bam M=$ID.dedup.qc REMOVE_DUPLICATES=true READ_NAME_REGEX='null' samtools view -h -q 30 -b $ID.dedup.bam > $ID.dedup.q30.bam macs2 callpeak -t ${chip}.dedup.q30.bam -c ${input}.dedup.q30.bam -n $chip -g mm --outdir $chip --cutoff-analysis -p 0.01 --call-summits -f BAMPE
Data quality	The number of peaks at FDR 5% and > 5-fold enrichment WT+DMF: 25142 KO+DMF: 29297 WT+NT: 1561 KO+NT: 1136
Software	bowtie2 version 2.4.9 samtools version 1.11 macs2 version 2.2.7.1

Flow Cytometry

Plots

Confirm that:

☒ The axis labels state the marker and fluorochrome used (e.g. CD4-FITC).

☒ The axis scales are clearly visible. Include numbers along axes only for bottom left plot of group (a 'group' is an analysis of identical markers).

☒ All plots are contour plots with outliers or pseudocolor plots.

☒ A numerical value for number of cells or percentage (with statistics) is provided.

Methodology

Sample preparation	Tumor tissues were weighted, cut into pieces and suspended with 10 ml tumor digestion buffer (2% FBS, 0.5 mg/ml collagenase IV and 100U/ml DNase I in RPMI medium). After digested for 45 minutes at 37°C under agitation (200 rpm) conditions, cell suspension was filtered using a 70-μm filter to obtain a single-cell suspension. Immune cells were isolated by density-gradient centrifugation using 40% and 80% Percoll (GE Healthcare). Then, tumor-infiltrating immune cells were stained using fluorescently labelled antibodies for FACS analysis.

Liver tissues were cut into pieces and suspended with 10 ml tumor digestion buffer (2% FBS, 0.5 mg/ml collagenase II, 0.5 mg/ml collagenase IV and 10U/ml DNase I in RPMI medium). After digested for 60 minutes at 37°C under agitation (200 rpm) conditions, cell suspension was filtered using a 70-µm filter to obtain a single-cell suspension. Immune cells were isolated by density-gradient centrifugation using 40% and 80% Percoll (GE Healthcare). Then, liver-infiltrating immune cells were stained using fluorescently labelled antibodies for FACS analysis.
Single-cell suspensions from the thymus, spleen and LNs were generated after mashing tissue through a 70-µm cell strainer. After treatment with red blood lysis buffer, cell suspensions were surface stained using fluorescently labeled antibodies for FACS analysis.
For intracellular staining of IFN and TNF, tumor single-cell suspensions were incubated in RPMI medium containing PMA (1:2000, MultiSciences, cat# CS0001), ionomycin (1:1000, MultiSciences, cat# CS0002), andBFA (1:1000, eBioscience, cat# 00-4506-51) for 4 hours at 37. After washing the samples with HBSS, surface proteins were stained, followed by fixation and permeabilization using the Cytofix/Cytoperm kit (eBioscience, cat# 85-88-8824-00), then staining of intracellular IFN and TNF.
For transcription factors staining, cells were fixed and permeabilized using the Foxp3/Transcription Factor Staining Buffer Set (eBioscience, cat# 00-5523-00), then staining of intranuclear TFs.

Instrument

Flow cytometry data was collected using Attune NxT flow cytometer (Thermo fisher).

Software

Flow cytometry data was analyzed using Flow Jo 10 software.

Cell population abundance

For flow cytometry analysis, 10^5 cells were stained in per sample.

Gating strategy

Cell size gating and doublet removal were applied respectively on the FSC-A/FCS-H. From the selected singlets, dead cells were discriminated out by gating on live/dead dye negative population. Then, from live cells, the CD4 T cells, CD8 T cells, B cells, NK cells, DCs, macrophages and monocytes and neutrophils were gated. For some experiments, IFN, TNF, Ki-67, T-BET, PD-1, TIM-3, TIGIT, TCF1, BCL-6, SCA-1 KLRG1 and CD127 were gated from CD8, CD44 and Kb-OVA triple positive cells. For surface marker, cytokine and transcriptional factor staining, isotype control antibodies were used to define background and non-specific binding signal.

☒ Tick this box to confirm that a figure exemplifying the gating strategy is provided in the Supplementary Information.